Modelling northern peatlands area and carbon dynamics since the Holocene with the ORCHIDEE-PEAT land surface model (SVN r5488)

Chunjing Qiu[1], Dan Zhu[1], Philippe Ciais[1], Bertrand Guenet[1], Shushi Peng[2], Gerhard Krinner[3], Ardalan Tootchi[4], Agnès Ducharne[4], Adam Hastie[5],

1. Laboratoire des Sciences du Climat et de l'Environnement, UMR8212, CEA-CNRS-UVSQ F-91191 Gif sur Yvette, France
2. Sino-French Institute for Earth System Science, College of Urban and Environmental Sciences, Peking University, 100871 Beijing, China
3. CNRS, Université Grenoble Alpes, Institut de Géosciences de l'Environnement (IGE), F-38000 Grenoble, France
4. Sorbonne Université, CNRS, EPHE, Milieux environnementaux, transferts et interaction dans les hydrosystèmes et les sols, Metis, F-75005 Paris, France
5. Department of Geoscience, Environment and Society, Université Libre de Bruxelles, 1050 Bruxelles, Belgium

Correspondence: Chunjing Qiu (chunjing.qiu@lsce.ipsl.fr)

Abstract

The importance of northern peatlands in the global carbon cycle has been recognized, especially for long-term changes. Yet, the complex interactions between climate and peatland hydrology, carbon storage and area dynamics make it challenging to represent these systems in land surface models. This study describes how peatland are included as an independent sub-grid hydrological soil unit (HSU) into the ORCHIDEE-MICT land surface model. The peatland soil column in this tile is characterized by multi-layered vertical water and carbon transport, and peat-specific hydrological properties. The cost-efficient version of TOPMODEL and the scheme of peatland initiation and development from the DYPTOP model, are implemented and adjusted, to simulate spatial and temporal dynamics of peatland. The model is tested across a range of northern peatland sites and for gridded simulations over the Northern Hemisphere (>30 °N). Simulated northern peatland area (3.9 million km^2), peat carbon stock (463 PgC) and peat depth are generally consistent with observed estimates of peatland area (3.4 – 4.0 million km^2), peat carbon (270 – 540 PgC) and data compilations of peat core depths. Our results show that both net primary production (NPP) and heterotrophic

respiration (HR) of northern peatlands increased over the past century in response to CO_2 and climate change. NPP increased more rapidly than HR, and thus net ecosystem production (NEP) exhibited a positive trend, contributing a cumulative carbon storage of 11.13 Pg C since 1901, most of it being realized after the 1950s.

1. Introduction

Northern peatlands carbon (C) stock is estimated between 270 and 540 PgC across an area of 3.4 – 4 million km^2 (Gorham, 1991; Turunen et al., 2002; Yu et al., 2010), amounting to approximately one-fourth of the global soil C pool (2000 – 2700 PgC) and one-half of the current atmospheric C pool (828 PgC) (Ciais et al., 2013; Jackson et al., 2017). Due to water-logged, acidic and low-temperature conditions, plant litter production exceeds decomposition in northern peatlands. More than half of northern peat carbon was accumulated before 7000 years ago during the Holocene (Yu, 2012). While being one of the most effective ecosystems at sequestering CO_2 from the atmosphere over the long-term, northern peatlands are one of the largest natural sources of methane (CH_4), playing a pivotal role in the global greenhouse gas balance (MacDonald et al., 2006; Mikaloff Fletcher et al., 2004; Smith, 2004).

The carbon balance of peatlands is sensitive to climate variability and climate change (Chu et al., 2015; Lund et al., 2012; Yu et al., 2003a). Projected climate warming and precipitation changes press us to understand the mechanisms of peat growth and stability, and further to assess the fate of the substantial amount of carbon stored in peatlands and its potential feedbacks on the climate. Several Land Surface Models (LSMs) have included representations of the biogeochemical and physical processes of peatlands to simulate the observed past extent and carbon balance of peatlands and predict their responses to future climate change (Chaudhary et al., 2017a, 2017b; Frolking et al., 2010; Kleinen et al., 2012; Spahni et al., 2013; Stocker et al., 2014; Wania et al., 2009a, 2009b; Wu et al., 2016). Water table is one of the most important factors controlling the accumulation of peat, because it limits oxygen supply to the saturated zone and reduces decomposition rates of buried organic matter (Kleinen et al., 2012; Spahni et al., 2013). It is highlighted by observed and experimental findings, that

variations in ecosystem respiration (ER) depend on water table depth (Aurela et al., 2007; Flanagan and Syed, 2011). However, some studies showed that changes in soil water content could be very small while the water table was lowering, the drawdown of the water table caused only small changes in soil air-filled porosity and hence exerted no significant effect on ER (Lafleur et al., 2005; Parmentier et al., 2009; Sulman et al., 2009). Therefore, while studying the interactions between peatland water and carbon balances, the dynamics of soil moisture deserves special attention.

The two-layered (acrotelm-catotelm) conceptual framework was chosen by many Earth System Models (ESMs) to describe peatland structures. The peat profile was divided into an upper layer with a fluctuating water table (acrotelm) and a lower, permanently saturated layer (catotelm) – using depth in relation to a drought water table or a constant value (a widely used depth is 0.3 m below the soil surface) as the discrete boundary of these two layers (Kleinen et al., 2012; Spahni et al., 2013; Wania et al., 2009a). This diplotelmic model assumes that all threshold changes in peatland soil ecological, hydrological and biogeochemical processes occur at the same depth, causing the lack of generality and flexibility in the model, and thus possibly hindering the representation of the horizontal and vertical heterogeneity of peatlands (Fan et al., 2014; Morris et al., 2011).

To our knowledge, only two models attempted to simulate peatland area dynamics for large-scale gridded applications (Kleinen et al., 2012; Stocker et al., 2014). Kleinen et al. (2012) modelled wetland extent and peat accumulation in boreal and arctic peatlands over the past 8000 years using the LPJ model. In their study, simulated summer mean, maximum and minimum wetland extent by TOPMODEL are used as surrogates for peatland area, from the assumption that peatland will only initiate and grow in frequently inundated areas. Stocker et al. (2014) extended the scope of Kleinen et al. (2012) in the DYPTOP model. In their model, soil water storage and retention were enhanced and runoff was reduced by accounting for peatland-specific hydraulic properties. A positive feedback on the local water balance and on peatland expansion was therefore exerted by peatland water table and peatland area fraction within a grid cell. Areas that are suitable for peatland development were distinguished from wetland

extent according to temporal persistency of inundation, water balance and peatland C balance. While both studies made pioneering progresses in the modelling of peatland ecosystems, they adopted a simple bucket approach to model peatland hydrology and peatland C accumulation, and neither of them resolved the diel cycle of surface energy budget.

To tackle these above-mentioned discrepancies and estimate the C dynamic as well as the peat area, we used the ORCHIDEE-MICT land surface model incorporating peatland as a sub-grid hydrological soil unit (HSU). The vertical water fluxes and dynamic carbon profiles in peatlands are simulated with a multi-layer scheme instead of a bucket model or a diplotelmic model (Sect. 2.1). Peatlands extent are modelled following the approach of DYPTOP (Stocker et al., 2014) but with some adaptions and improvements (Sect. 2.2). The aim of this study is to model the spatial extent of northern peatlands since the Holocene and to reproduce peat carbon accumulation over the Holocene.

2. Model description

ORCHIDEE-MICT is an updated version of the ORCHIDEE land surface model with an improved and evaluated representation of high-latitude processes. Phase changes of soil water (freeze/thaw), three-layered snowpack and its insulating effects on soil temperature in winter, permafrost physics and its impacts on plant water availability and soil carbon profiles are all represented in this model (Guimberteau et al., 2018). Based on ORCHIDEE-MICT, ORCHIDEE-PEAT is specifically developed to dynamically simulate northern peatland extent and peat accumulation. ORCHIDEE-PEAT version 1 was evaluated and calibrated against eddy-covariance measurements of CO_2 and energy fluxes, water table depth, as well as soil temperature from 30 northern peatland sites (Qiu et al., 2018). Parameterizations of peatland vegetation and water dynamics are unchanged from ORCHIDEE-PEAT version 1: Vegetations growing in peatlands are represented by one C3 grass plant functional type (PFT) with shallow roots (see dedicated section 2.2.1 of Qiu et al. (2018) for additional discussion on peatland PFT); Surface runoff of non-peatland areas in the grid cell is routed into peatland; Vertical water fluxes in peatland tile is modelled with peat-specific hydraulics

126 (Text S1 in the Supplement). Here, we improve peatland C dynamics by replacing the

127 diplotelmic peatland C model with a multi-layered one. The 32-layered thermal and C

128 models in the standard ORCHIDEE-MICT is used to simulate peatland C accumulation

129 and decomposition (Sect. 2.1). With fine resolution in the soil surface (10 layers for the

130 top 1m), this 32-layer model better represents the effects of soil temperature, soil

131 freezing, and soil moisture on carbon decomposition continuously within the peat

132 profile than a diplotelmic model. Furthermore, the approach proposed by Stocker et al.

133 (2014) is incorporated into the model to simulate dynamics of peatland area (Sect. 2.2).

134 This model simulating the dynamics of peatland extent and the vertical buildup of peat

135 is hereinafter referred to as ORCHIDEE-PEAT v2.0. It is worth mentioning that

136 Guimberteau et al. (2018) defined soil thermal properties of a specific grid cell as the

137 weighted average of mineral soil and pure organic soil in that grid, with C content of

138 the grid cell derived from the soil organic C map from NCSCD (Hugelius et al., 2013)

139 and HWSD (FAO et al., 2012). This development makes it possible to include the

140 impacts of peat carbon on the gridcell soil thermics, and is activated in this study.

141 **2.1 Modeling peat accumulation and decomposition**

142   The model has two litter C pools (metabolic and structural) and three soil C pools

143 (active, slow and passive); all pools are vertically discretized into 32 layers, with

144 exponentially coarser vertical resolution as depth increases and a total depth of 38 m.

145 Decomposition of the C in each pool and the C fluxes between the pools are calculated

146 at each layer, with each pool having a distinct residence time. A detailed description of

147 the litter and soil C pools and carbon flows between them can be found in the

148 Supplement Text S2.

149 **2.1.1   Peat carbon decomposition**

150 Decomposition of peat soil C is calculated at each layer, controlled by base

151 decomposition rates of different pools modified by soil temperature, moisture and depth:

152 $k_{i,l} = k_{0,i} \times f_{T,l} \times f_{M,l} \times f_{Z,l}$,   (1)

153 where $k_{i,l}$ is the decomposition rate of the pool i at layer l, $k_{0,i}$ is the base

154 decomposition rate of pool i, $f_{T,l}$ is the temperature modifier at layer l, $f_{M,l}$ is the

155 moisture modifier, $f_{Z,l}$ is a depth modifier that further reduces decomposition at depth.

For unfrozen soils, the temperature modifier is an exponential function of soil temperature, while below 0℃ when liquid water enabling decomposition disappears, respiration linearly drops to zero at −1℃ (Koven et al., 2011). The soil moisture modifier is prescribed from the meta-analysis of soil volumetric water content ($m^3 m^{-3}$) - respiration relationship for organic soils conducted by Moyano et al. (2012). See Supplement Text S3 for a more detailed description of the temperature and moisture modifier.

Following Koven et al. (2013), we implement a depth modifier ($f_{Z,l}$) to represent unresolved depth controls (i.e. priming effects, sorption of organic molecules to mineral surfaces) on C decomposition. This depth modifier decreases exponentially with depth:

$$f_{Z,l} = \exp\left(-\frac{z_l}{z_0}\right) , \tag{2}$$

where z_l (m) is the depth of the layer l, z_0 (m) is the e-folding depth of base decomposition rate.

2.1.2 Vertical buildup of peat

Water-logging and cold temperature in northern peatland regions prevent complete decomposition of dead plant material, causing an imbalance between litter production and decay (Parish et al., 2008). The un-decomposed plant residues accumulate as peat, and consequently, the peat surface shows an upward growth. Instead of modeling this upward accumulation of peat, we simulate a downward movement of C by adapting the method that Jafarov and Schaefer (2016) used to build up a dynamic surface organic layer.

From 102 peat cores from 73 sites (Lewis et al., 2012; Loisel et al., 2014; McCarter and Price, 2013; Price et al., 2005; Tfaily et al., 2014; Turunen et al., 2001; Zaccone et al., 2011), we compiled bulk density (BD) measurements into depth bins which correspond to the top 17 soil layers (~8.7 m) of the model (Fig. S1a). The median observed bulk density at each depth bin is assigned to the corresponding soil layer of the model (BD_l). For deeper soil layers of the model (18th - 32th), the value of the 17th soil layer is used. The fraction of C (% weight) of each soil layer (α_{cl}) is derived from a regression with bulk density from 39 cores from 29 sites (Fig. S1b). With these data,

185   we calculate the empirical amount of C that each soil layer can hold:

186    $M_l = BD_l \times \alpha_{cl} \times \Delta Z_l$,   (3)

187   where BD_l (kg m^{-3}) is the soil bulk density of layer l, α_{cl} is the mass fraction of

188   carbon in the soil, and ΔZ_l (m) is the thickness of the layer.

189   We then model the vertical downward movement of C between soil layers to mimic

190   the aggradation of carbon in the peat as follows: If carbon in layer l (C_l) exceeds a

191   maximum amount ($M_{th,l}$), a prescribed fraction (f) of the carbon is moved to the layer

192   below ($l+1$). Here, the carbon flux from layer l to the layer below ($l+1$) is calculated

193   as:

194    $flux_{l \to l+1} = \begin{cases} 0, & C_l < M_{th,l} \\ f \times C_l & C_l \geq M_{th,l} \end{cases}$,   (4)

195   where C_l (kg m^{-2}) is the carbon content of layer l. The threshold amount of carbon

196   in layer l ($M_{th,l}$) is a prescribed fraction (f_{th}) of the empirically determined M_l:

197    $M_{th,l} = f_{th} \times M_l$,   (5)

198   The values of model parameters f and f_{th} do not change with soil depth.

199   Finally, the total peat depth is defined as the depth that carbon can be transferred to:

200    $H = \dfrac{C_k}{M_k} \times \Delta Z_k + \sum_{i=1}^{k-1} \Delta Z_i$,   (6)

201   where k is the deepest soil layer where carbon content is greater than 0, C_k (kg m^{-2})

202   is the carbon content of layer k, M_k (kg m^{-2}) is empirical amount of carbon that layer

203   k can hold, and ΔZ_k (m) is the thickness of layer k.

204   **2.2 Simulating dynamic peatland area extent**

205   In grid-based simulations, each grid cell is characterized by fractional coverages of

206   PFTs. The dynamic coverage of each non-peatland PFT is determined by the DGVM

207   equations as functions of bioclimatic limitations, sapling establishment, light

208   competition and natural plant mortality (Krinner et al., 2005; Zhu et al., 2015). Here, a

209   cost-efficient TOPMODEL from the DYPTOP model (Stocker et al., 2014) is

210   incorporated, and calibrated for each grid cell by present-day wetland area that are

211   regularly inundated or subject to shallow water tables, to simulate wetland extent (Sect.

212   2.2.1). Then, the criteria for peatland expansion is adapted from DYPTOP to distinguish

213 peatland from wetland (Sect. 2.2.2).

2.2.1 The cost-efficient TOPMODEL

215 Concepts of TOPMODEL (Beven and Kirkby, 1979) have been proven to be effective
216 at outlining wetland areas in current state-of-the-art LSMs (Kleinen et al., 2012;
217 Ringeval et al., 2012; Stocker et al., 2014; Zhang et al., 2016). Based on TOPMODEL,
218 sub-grid-scale topography information and soil properties of a given watershed / grid
219 cell are used to redistribute the mean water table depth to delineate the extent of sub-
220 grid area at maximum soil water content. The empirical relationship between the
221 flooded fraction of a grid cell and the grid cell mean water table position ($\overline{WT}$) can be
222 established (Fig. 1a) and approximated by an asymmetric sigmoid function, which is
223 more computationally efficient than determining water table depth for each sub-grid
224 pixel (Stocker et al., 2014). Here, we adopted the cost-efficient TOPMODEL from
225 Stocker et al. (2014) and calibrated TOPMODEL parameters for each grid cell to match
226 the spatial distribution of northern wetlands (see more details in Text S4). Tootchi et al.
227 (2019) reconciled multiple current wetland datasets and generated several high-
228 resolution composite wetland (CW) maps. The one used here (CW-WTD) was derived
229 by combining regularly flooded wetlands (RFW), which is obtained by overlapping
230 three open-water and inundation datasets (ESA-CCI (Herold et al. 2015), GIEMS-D15
231 (Fluet-Chouinard et al., 2015), and JRC (Fluet-Chouinard et al., 2015)), with areas that
232 have shallow (WT $\leq$ 20cm) water tables from groundwater modeling of Fan et al.
233 (2013). CW-WTD wetlands are static and aim at representing the climatological
234 maximum extent of active wetlands and inundation. We therefore compare simulated
235 maximum monthly mean wetland extent over 1980−2015 with CW-WTD to calibrate
236 TOPMODEL parameters. Note that lakes from the HydroLAKES database have been
237 excluded from the CW-WTD map because of their distinct hydrology and ecology
238 compared with wetlands (Tootchi et al., 2019).

2.2.2 Peatland development criteria

240 The criteria used to constrain peatland area development are greatly inspired by
241 DYPTOP (Stocker et al., 2014), but with some adaptions.

242   The initiation of peatland only depends on moisture conditions of the grid cell (Fig.

1b ③ – ⑦): First, only the sub grid cell area fraction that is frequently inundated has the potential to become peatland (f_{pot}). Stocker et al. (2014) introduced a 'flooding persistency' parameter (N in Eq.12, Eq.13 in Stocker et al. (2014)) for the DYPTOP model to represents the temporal frequency of inundation. N is a globally uniform parameter in DYPTOP, being set to 18 months during the preceding 31 years. However, the formation of peat is a function of local climate, and thus suitable formation conditions for peatland vary between geographic regions. To be specific, the accumulation of peat in arctic and northern latitudes is due both to high water table and to low temperature, while it is mainly a result of water-logging conditions in sub-tropical and tropical latitudes (Parish et al., 2008). Therefore, it is essential to apply different values for the 'flooding persistency' parameter for different regions, according to local climate conditions. We re-defined the requirement of persistent flooding for peatland formation as: the area fraction that has the potential to become peatland needs to be flooded at least *Num* months during the preceding 30 years, with *Num* being the total number of growing season months (monthly air temperature > 5 °C) in 30 years (Fig. 1b ⑤). In this case, with the help of relatively low air temperature making shorter growing seasons, arctic and boreal latitudes need shorter inundation periods than sub-tropical and tropical regions to form peatland. Furthermore, as *Sphagnum*-dominated peatlands are sensitive to summer moisture conditions (Alexandrov et al., 2016; Gignac et al., 2000), the summer water balance of the grid cell needs to pass a specific threshold (*SWB*) to form peat and to achieve the potential peatland area (Fig. 1b ⑦). The summer water balance is calculated as the difference between total precipitation (P) and total potential evapotranspiration (PET) of May-September. We consider *SWB* as a tunable parameter in the model and run simulations with $SWB = -6$ cm, 0 cm, 3 cm, and 6 cm. $SWB = 6$ cm is selected so that the model captures the southern frontier of peatland in Eurasia and western North America (Text S5). Note that the definition of summer (May-September) and *SWB* are not applicable for tropical regions and the Southern Hemisphere.

After the initiation, the development of peatland area is controlled by both moisture conditions of the grid cell and the long-term carbon balance of the peatland HSU (Fig.

1c ⑨ − ⑰). If the climate becomes drier and the calculated potential peatland area is smaller than the current peatland area, the peatland HSU area will contract to the new potential peatland area fraction (Fig. 1c ⑫). Otherwise (Fig. 1c ⑬), the peatland has the possibility to expand when the summer water balance threshold is passed. If these above criteria are satisfied, the final decision depends on the carbon density of the peatland (C_{peat}): the peatland can expand only when long-term input exceeds decay and a certain amount of C (C_{lim}) has accumulated (Fig. 1c ⑰). C_{lim} is defined here as long-term peatland C balance condition, it's a product of a mean measured peat depth (1.07 m) from 40 peat cores (with peat age greater than 1.8 ka but smaller than 2.2 ka) from North American peatland (Gorham et al., 2007, 2012) and from the West Siberian lowlands (Kremenetski et al., 2003), a dry bulk density assumption of $100.0 \, \text{kg m}^{-3}$ and a mean C fraction of 47% in total peat (Loisel et al., 2014). Our estimation for C_{lim} is $50.3 \, \text{kg C m}^{-2}$, matches well with the C density criterion ($50 \, \text{kg C m}^{-2}$) chosen by Stocker et al. (2014) to represent typical peatland soil.

The moisture conditions are evaluated every month throughout the simulation, while C_{peat} is checked only in the first month after the SubC in Spin-up1 and is checked every month in Spin-up2 and the transient simulation (see Sect. 3.2). The peatland area fraction (f_{peat}) is updated every month. During the simulation, the contracted area and C are allocated to an 'old peat' pool and are kept track of by the model. It should be noted that drainage (drought) may cause decrease of porosity and saturated moisture content of peat soils (Oleszczuk and Truba, 2013) and, changes in peatland vegetation compositions (Benavides, 2014). But the current model structure doesn't allow us to take these potential changes in peatland into consideration. Therefore, parameterizations of the "old peat" pool is identical to mineral soils, following the study of Stocker et al. (2014). When peatland expansion happens, the peatland will first expand into this 'old peat' area and inherit its stored C (Stocker et al., 2014).

The difference between our model and the DYPTOP model in simulating peatland area dynamics can be summarized as follows: (1) TOPMODEL calibration: TOPMODEL parameters are globally uniform in the DYPTOP model, but grid cell-specific in ORCHIDEE-PEAT v2.0. (2) Criteria for peatland expansion: In the

DYPTOP, the "flooding persistency" parameter is globally uniform, being 18 months in the preceding 31 years. And the ecosystem water balance is expressed as annual precipitation-over-actual-evapotranspiration (POAET). In ORCHIDEE-PEAT v2.0, the flooding persistency parameter is grid cell-specific, being the total number of growing season months in the preceding 30 years. And peatland expansion is limited only by summer water balance. The relative areal change of peatland is limited to 1% per year in DYPTOP, but not limited in our model. (3) Peatland initiation: DYPTOP prescribes a very small peatland area fraction (0.001%) in each grid cell to simulate peatland C balance condition. Peatland can expand from this "seed" once water and carbon balance criteria are met. In ORCHIDEE-PEAT v2.0, no "seed" is needed because only the flooding persistency and summer water balance criteria need to be met for the first initiation of peatland (Fig. 1b), carbon balance is only checked after initiation (Fig.1c).

3. Simulation setup and evaluation datasets

3.1 Critical model parameters

The base decomposition rates of active, slow and passive peat soil carbon pools in the model are 1.0 a^{-1}, 0.027 a^{-1} and 0.0006 a^{-1} at reference temperature of 30 °C, respectively (Table 1, Sect. 5: Choice of model parameters). The e-folding depth of the depth modifier (z_0, Eq. 2) determines the general shape of increases of soil C turnover time with depth; the prescribed threshold to allow downward C transfer between soil layers (f_{th}, Eq. 5) and the prescribed fraction of C to be transferred (f, Eq. 4) determine movement and subsequent distribution of soil C along the soil profile. We compare simulated C vertical profiles with observed C profiles at 15 northern peatland sites (Table S1) (Loisel et al., 2014) using different combinations of parameters ($z_0 = (0.5, 1.0, 1.5, 2.0)$, $f_{th} = (0.5, 0.7, 0.9)$ and $f = (0.1, 0.2, 0.3)$) and eventually selected $z_0 = 1.5\, m$, $f_{th} = 0.7$ and $f = 0.1$ based on visual examinations to match the observed C content. Model sensitivity to the selection will be discussed in Sect. 5.

3.2 Simulation protocol

We conduct both site-level and regional simulations with ORCHIDEE-PEAT v2.0 at 1° × 1° spatial resolution. Regional simulations are performed for the Northern Hemisphere (>30° N), while site-level simulations are performed for 60 grid cells

containing at least one peat core (Table S1, Fig. S2). Peat cores used in site-level simulations are from the Holocene Perspective on Peatland Biogeochemistry database (HPPB) (Loisel et al., 2014). Both site-level and regional simulations are forced by the 6-hourly meteorological forcing from the CRUNCEP v8 dataset, which is a combination of the CRU TS monthly climate dataset and NCEP reanalysis (https://vesg.ipsl.upmc.fr/thredds/catalog/store/p529viov/cruncep/V7_1901_2015/catalog.html).

All simulations start with a two-step spin-up followed by a transient simulation after the pre-industrial period (Fig. S3). The first spin-up (Spin-up1) includes N cycles of a peat carbon accumulation acceleration procedure consisting of 1) 30 years with the full ORCHIDEE-PEAT (FullO) run on 30 min time step followed by 2) a stand-alone soil carbon sub-model (SubC) run to simulates the soil carbon dynamics in a cost effectively way on monthly steps (fixed monthly litter input, soil water and soil thermal conditions from the preceding FullO simulation). Repeated 1961−1990 climate forcing is used in Spin-up1 to approximate the higher Holocene temperatures relative to the preindustrial period (Marcott et al., 2013). The atmospheric CO_2 concentration is fixed at the preindustrial level (286 ppm). Each time we run the SubC for 2000 years (2 ka) in the first $N-1$ sets of acceleration procedures while, the value of N and the time length of the last set of acceleration procedure (X) are defined according to the age of the peat core in site-level simulations, and are defined according to the reconstructed glacial retreat in regional simulations (Fig. S4, S5). The reconstructed glacial retreat used in this study are from Dyke (2004) for North America and are from Hughes et al. (2016) for Eurasia (Text S6).

In the second spin-up step (Spin-up2), the full ORCHIDEE-PEAT model was run for 100 years, forced by looped 1901−1920 climate forcing and preindustrial atmospheric CO_2 concentration so that physical and carbon fluxes can approach to the preindustrial equilibrium. After the two spin-ups, a transient simulation is run, forced by historical climate forcing from CRUNCEP and rising atmospheric CO_2 concentration. For site-level simulations, the transient period starts from 1860 and ends at the year of coring (Table S1). For regional simulations, the transient period starts from 1860 and ends at

2009.

3.3 Evaluation datasets

3.3.1 Evaluation datasets for site-level simulations

All peatland sites used in this study are from the HPPB database (Loisel et al., 2014). All the peat cores measured peat ages and depths (60 sites, Table S1), hence are used to evaluate simulated peat depth, with sites being grouped into different peatland types, climate zones and ages. For peat cores where peat ages, depths, fraction of C and bulk density were recorded (15 sites marked in red in Table S1), we construct vertical C profiles with this measured information to compare with our simulated C profiles.

3.3.2 Northern peatland evaluation datasets for regional simulations

Area

Simulated peatlands area in 2009 is evaluated against: 1. World Inventory of Soil Emission potentials (WISE) database (Batjes, 2016); 2. An improved global peatland map (PEATMAP) by reviewing a wide variety of global, regional and local scale peatland distribution information (Xu et al., 2018); 3. International Mire Conservation Group Global Peatland Database (IMCG-GPD) (Joosten, 2010); 4. Peatland distribution map by Yu et al. (2010).

Soil organic carbon stocks

Simulated peatlands SOC is evaluated against: 1. The WISE database (Batjes, 2016); 2. The IMCG-GPD (Joosten, 2010).

All the above-mentioned datasets used to evaluate ORCHIDEE-PEAT v2.0 at regional scale are described in the Supplement Text S7.

Peat depth

Gorham et al. (2007, 2012) and Kremenetski et al. (2003) collected depth and age of 1685 and 130 peat cores, respectively, from literature data on peatlands in North America (NA) and in the West Siberian lowlands (WSL). These compilations make it possible for us to validate peat depths simulated by ORCHIDEE-PEAT v2.0 at regional scales, in addition to the detailed site-runs in Sect. 3.3.1. Compared to the HPPB database, these datasets lack detailed peat properties (i.e. C content, peatland type…), but contain more samples and cover larger areas. Note that as this study aims to

reproduce development of northern peatlands since the Holocene, peat cores that are older than 12 ka are removed from the model evaluation. At last, 1521 out of 1685 observed peat cores in NA, 127 out of 130 observed peat cores in WSL, are used in model evaluation (Sect. 4.2: Peat depth).

4. Results

4.1 Site simulation

We first evaluate the performance of ORCHIDEE-PEAT v2.0 in reproducing peat depths and vertical C profiles at the 60 sites from HPPB (Table S1). Out of the 60 grid cells (each grid cell corresponding to one peat core), ORCHIDEE-PEAT v2.0 produces peatlands in 57 of them. The establishment of peatlands at Zoige, Altay and IN-BG-1 (Table S1) is prevented in the model by the summer water balance criterion of these grid cells. Peat depths are underestimated for most sites (Fig. 2). Simulated depth of these 57 sites ranges from 0.37 m to 6.64 m and shows a median depth of 2.18 m, while measured peat depth ranges from 0.96 to 10.95 m, with the measured median depth being 3.10 m (Table 2). The root mean square error (RMSE) between observations and simulations is 2.45 m.

The measured and simulated median peat depths for the 14 fen sites are 3.78 m and 2.16 m, compared to 3.30 m and 2.18 m, respectively for the 33 bog sites (Table 2). The model shows slightly higher accuracy for fens than for bogs, with RMSE for fens being 2.08 m and 2.59 m for bogs. RMSE for peat depths of sites that are older than 8 ka are greater than that of younger sites, but are smaller than the measured mean depth (3.5 m) of all peat cores. Simulated median depth of the 6 arctic sites are larger than observations, but that of the 47 boreal sites and the 4 temperate sites are smaller than observations (Table 2). The RMSE for temperate sites is larger than that for arctic or boreal sites.

The simulated and observed vertical profiles of soil C for the 15 sites are shown in Fig. 3, simulated C concentrations are generally within the range of measurements at most of the sites, but are underestimated at Sidney bog, Usnsk Mire 1, Lake 785 and Lake 396. In the model, the buildup of peat is parameterized by downward movement of C between soil layers, with the maximum amount of C that each layer can hold being

calculated from median observed bulk density and C fraction of peat core samples (Sect. 2.1.2). High C concentration of cores that have significantly larger bulk density and / or C fraction than the median of the measurements thus cannot be reproduced. This is the case of Lake 785 and Lake 396 (Table S1), where C concentrations are underestimated and depths are overestimated (Fig. 2), while simulated total C content is close to observations (for Lake 785, measured and simulated C content is 86.14 $kgC\ m^{-2}$ and 96.13 $kgC\ m^{-2}$, respectively, while values for Lake 396 are 57.2 and 70.2 $kgC\ m^{-2}$).

As shown in Fig. 4, there is considerable variability in depth and C concentration profiles among peat cores within a grid cell, even though these cores have a similar age. We rerun the model at the 5 grid cells where more than one peat core has been sampled, with time length of the simulation being defined as the mean age of cores in the same one grid cell. The simulated peat depth and C concentration profiles at G2, G4, and G5 are generally within the range of peat core measurements (Fig. 4). Observed C fraction at grid cell G1 and G3 are much greater than the median value of all peat core samples (Sect. 2.1.2), thus simulated C concentration along the peat profile are smaller than observations, but peat depth are still overestimated by the model. As it is the case with Lake 785 and Lake 396.

4.2 Regional simulation

Northern peatlands area and C stock

Simulated maximum inundated area of the Northern Hemisphere is 9.1 million km^2, smaller than the wetland areas in CW-WTD (~13.2 million km^2 after excluding lakes). TOPMODEL gives an area fraction at maximum soil water content while CW-WTD includes both areas seasonally to permanently flooded and areas that are persistently saturated or near-saturated (the maximum water table shallower than 20 cm) soil-surface. Therefore, an exact match between CW-WTD and the model prediction is not expected. The model generally captures the spatial pattern of wetland areas represented by CW-WTD (Fig. 5). The multi-sensor satellite-based GIEMS dataset (Prigent et al., 2007, 2012) which provides observed monthly inundation extent over the period of 1993 − 2007 is used to evaluate simulated seasonality of inundation. Fig. 6 shows that

the seasonality of inundation is generally well captured by the model, although simulated seasonal maximum of inundation extent occurs earlier than observations (except in WSL) and simulated duration of inundation is longer than observations.

While our model predicts the natural extent of peatlands under suitable climate conditions, soil formation processes and soil erosion are not included in the model. We mask grid cells that are dominated by Leptosols, which are shallow or stony soils over hard rock, or highly calcareous material (Nachtergaele, 2010) (Fig. S6, Fig. S7). Peatlands have been extensively used for agriculture after drainage and / or partial extraction worldwide (Carlson et al., 2016; Joosten, 2010; Leifeld and Menichetti, 2018; Parish et al., 2008). Intensive cultivation practices might cause rapid loss of peat C and ensuing disappearance of peatland. Additionally, agricultural peatlands are often classified as cropland, not as organic soils (Joosten, 2010). Therefore, we mask agricultural peatland from the results by assuming that crops occupy peatland in proportion to the grid cell peatland area (Carlson et al., 2016). The distribution and area of cropland used here is from the MIRCA2000 data set (Portmann et al., 2010), which provides monthly crop areas for 26 crop classes around the year 2000 and includes multicropping explicitly (Fig. S8). After masking Leptosols and agricultural peatlands from the simulated peatland areas and peatland C stocks, the simulated total northern peatlands area is 3.9 million km^2 ($f_{noLEP-CR}$, Fig. 7d), holding 463 PgC ($C_{noLEP-CR}$, Fig. 8b). These estimates fall well within estimated ranges of northern peatland area (3.4 – 4 million km^2) and carbon stock (270 – 540 PgC) (Gorham, 1991; Turunen et al., 2002; Yu et al., 2010). Simulated peatland area matches relatively well with PEATMAP data in Asian Russia but overestimates peat area in European Russia (Table 3). The simulated total peatlands area of Canada is in relatively good agreement with the three evaluation data sets, though the world's second largest peatland complex at the Hudson Bay lowlands (HBL) is underestimated and a small part of the northwest Canada peatlands is missing. Packalen et al. (2014) stressed that initiation and development of HBL peatlands are driven by both climate and glacial isostatic adjustment (GIA), with initiation and expansion of HBL peatlands tightly coupled with land emergence from the Tyrrell Sea, following the deglaciation of the Laurentide ice sheet and under suitable

483   climatic conditions. The pattern of peatlands at southern HBL was believed to be driven

484   by the differential rates of GIA rather than climate (Glaser et al., 2004a, 2004b). More

485   specifically, Glaser et al. (2004a, 2004b) suggested that the faster isostatic uplift rates

486   on the lower reaches of the drainage basin reduce regional slope, impede drainage and

487   shift river channels. Our model, however, can't simulate the tectonic and hydrogeologic

488   controls on peatland development. In addition, the development of permafrost at depth

489   as peat grows in thickness over time acts to expand peat volume and uplift peat when

490   liquid water filled pores at the bottom of the peat become ice filled pores (Seppälä,

491   2006). This process is not accounted for in the model and may explain why the HBL

492   does not show up as a large flooded area today whereas peat developed in this region

493   during the early development stages of the HBL complex. The simulated distribution

494   of peatland area in Alaska agrees well with Yu et al. (2010) and WISE. There is a large

495   overestimation of peatland area in southeastern US (Table 3, Fig. 7d). The simulated

496   peat C stock in Russia (both the Asian and the European part), and in US are

497   overestimated compared to IMCG-GPD and WISE, but that of Canada is

498   underestimated (Table 4, Fig. 8b).

499   **Peat depth**

500   Fig. 9 shows measured and simulated peat depth in NA and WSL. Some peat cores are

501   sampled from the Canadian Arctic Archipelago, southwestern US and the northern tip

502   of Quebec, where there is no peatland in peat inventories / the soil database. These sites

503   support the notion that the formation and development of peatland are strongly

504   dependent on local conditions, i.e. retreat of glaciers, topography, drainage, vegetation

505   succession (Carrara et al., 1991; Madole, 1976). As a large-scale LSM, the model can't

506   capture every single peatland: 429 out of 596 grid cells that contain observed peat cores

507   in NA are captured by the model, while the model simulates peatlands in 54 out of 60

508   observed grid cells in WSL. Cores that are not captured by the model are removed from

509   further analysis (319 out of 1521 peat cores in NA, 18 out of 127 peat cores in WSL,

510   are removed).

511   As shown in Fig. 4, within a grid cell, sampled peat cores can have very different

512   depths and / or ages. We calculate the mean depth of cores in each of the grid cells and

513   compare it against the simulated mean depth. The mean age of cores in each of the grid

514   cells is used to determine which output of the model should be examined. For instance,

515   the mean age of the four cores in grid cell (40.5 °N, 74.5 °W) is 2.5 ka, and accordingly,

516   we pick out the simulated depth of this grid cell right after the first run of SubC (Fig.

517   S3) to compare with the mean depth of these cores. We acknowledge that this is still a

518   crude comparison since the simulation protocol implies that we can only make the

519   comparison at 2000-year intervals. Nonetheless, it is a compromise between running

520   the model for 1815 peat cores independently and comparing the mean depth of

521   measured points with grid-based simulated depth. As shown in Fig. 10, for each age

522   interval (of both the West Siberian lowlands and North America), the variation in

523   simulated depth is smaller than that in the measurement. The two deepest simulated

524   peat in WSL belong to the fourth age group ($6 < Age \leq 8$ ka) and are the result of a

525   shallow active layer; while C is moving downward to deeper and deeper layers, the

526   decomposition is greatly limited by cold conditions at depth. At both WSL and NA,

527   simulated median peat depths ($2.07 - 2.36$ m at WSL, $1.02 - 2.15$ m at NA) are in

528   relatively good agreement with measurements ($1.8 - 2.31$ m at WSL, $0.8 - 2.46$ m at

529   NA) for cores younger than 8 ka (Fig. 10). For the two oldest groups (peat age > 8 ka),

530   the simulated median depths are about 0.70 m shallower than measurements at NA and

531   about 1.04 m shallower at WSL.

Undisturbed northern peatland carbon balance in the past century

533   Simulated mean annual (averaged over $1901 - 2009$) net ecosystem production (NEP)

534   of northern peatlands varies from $- 63$ gC m^{-2} a^{-1} to 46 gC m^{-2} a^{-1} (Fig. 11). The West

535   Siberian lowlands, the Hudson Bay lowlands, Alaska, and the China-Russia border are

536   significant hotspots of peatland C uptake. Simulated mean annual NEP of all northern

537   peatlands over $1901 - 2009$ is 0.1 PgC a^{-1}, consistent with the previous estimate of

538   0.076 PgC a^{-1} by Gorham (1991) and the estimate of 0.07 PgC a^{-1} by Clymo et al.

539   (1998). From 1901 to 2009, both simulated net primary production (NPP) and simulated

540   heterotrophic respiration (HR) show an increasing trend, but NPP rises faster than HR

541   during the second half of the century (Fig. 12a). The increase of NPP is caused by

542   atmospheric CO_2 concentration and increasing of air temperature (Fig. 12, Fig. S9). As

543 air (soil) temperature increases, HR also increases but lags behind NPP (Fig. 12, Fig.

544 S9). Simulated annual NEP ranges from –0.03 PgC a^{-1} to 0.23 PgC a^{-1}, with a

545 significant positive trend over the second half of the century (Fig. 12b). NEP shows a

546 significant positive relationship with air (soil) temperature and with atmospheric CO_2

547 concentration (Fig. S9). CH_4 and dissolved organic carbon (DOC) are not yet included

548 in the model, both of them are significant losses of C from peatland (Roulet et al., 2007).

549 **5. Discussion**

550 **Peat depth**

551 We found a general underestimation of peat depth (Fig. 2, Fig. 10), possibly due to the

552 following reasons. Firstly, there is a lack of specific local climatic and topographic

553 conditions: The surfaces of peatlands are mosaics of microforms, with accumulation of

554 peat occurring at each individual microsites of hummocks, lawns and hollows.

555 Differences in vegetation communities, thickness of the unsaturated zone, local peat

556 hydraulic conductivity and transmissivity between microforms result in considerable

557 variation in peat formation rate and total C mass (Belyea and Clymo, 2001; Belyea and

558 Malmer, 2004; Borren et al., 2004; Packalen et al., 2016). Cresto Aleina et al. (2015)

559 found that the inclusion of microtopography in the Hummock-Hollow model delayed

560 the simulated runoff and maintained wetter peat soil for a longer time at a peatland of

561 Northwest Russia, thus contributed to enhanced anoxic conditions. Secondly, site-

562 specific parameters are not included in gridded simulations: Parameters describing peat

563 soil properties, i.e., soil bulk density and soil carbon fraction, determine the amount of

564 C that can be stored across the vertical soil profile. Hydrological parameters, i.e., the

565 hydraulic conductivity and diffusivity, and the saturated and residual water content,

566 regulate vertical fluxes of water in the peatland soil and expansion/contraction of the

567 peatland area, and hence influence the decomposition and accumulation of C at the sites

568 considered. Plant trait parameters, i.e. the maximal rate of carboxylation (V_{cmax}), the

569 light saturation rate of electron transport (J_{max}) determine the carbon budgets of the sites

570 (Qiu et al., 2018). The depth modifier, which parameterizes depth dependence of

571 decomposition, controls C decomposition at depth and is an important control on

572 simulated total C and the vertical C profile. A third reason is sample selection bias:

Ecologists and geochemists tend to take samples from the deepest part of a peatland complex to obtain the longest possible records (Gorham, 1991; Kuhry and Turunen, 2006). In contrast, the model is designed to model an average age and C stock of peatlands in a grid location and thus preferably, the simulated C concentrations of a grid cell should only be validated against grids represented by a number of observed cores. We do try to compare the model output with multiple peat cores (Fig. 4, Fig. 10), but we need to note that shallow peats are not sufficiently represented in field measurements. A fourth source of error is that simulated initiation time of peat development at some sites are too late compared to ages of measured cores: The model multiple spin-up strategy accounts for coarse-scale ice-sheet distribution at discrete Holocene intervals (Sect. 3.2, Fig. S3), and if the modelled occurrence of peatland is too late, the accumulated soil C may be underestimated. For example, at the Patuanak site, where the core age is 9017 a, the model was run with 4 times' SubC (Table S1). However, there was no peatland before the first SubC, meaning that simulated peatland at this grid cell was 2000 years younger than the observation and that our simulation missed C accumulation during the first 2000 years at this site. This may be another source of bias associated with the model resolution, namely that local site conditions fulfilled the initiation of peatland at specific locations, but the average topographic and climatic conditions of the coarse model grid cell were not suitable for peatland initiation. Also, one has to keep in mind that a single / a few sample (s) from a large peat complex may not be enough to capture the lateral spread of peat area, which may be an important control on accumulation of C (Charmen, 1992; Gallego-Sala et al., 2016; Parish et al., 2008). The underestimation of peat depth can also come from biased climate input data: Spin-ups of the model are forced with repeated 1961−1990 climate, assuming that Holocene climate is equal to recent climate. While peatland carbon sequestration rates are sensitive to climatic fluctuations, centennial to millennial scale climate variability, i.e. cooling during the Younger Dryas period and the Little Ice Age period, warming during the Bølling-Allerød period are not included in the climate forcing data (Yu et al., 2003a, 2003b). An early Holocene carbon accumulation peak was found during the Holocene Thermal Maximum when the climate was warmer than present (Loisel et al.,

2014; Yu et al., 2009). Finally, effects of landscape morphology on drainage as well as drainage of glacial lakes are not incorporated and can represent a source of uncertainty.

Vertical profiles of peatland soil organic carbon

We note that caution is needed in interpreting the comparison between simulated peat C profile and measured C profile from peat cores (Fig. 3, Fig. 4). In reality, peat grow both vertically and laterally since inception, with the peat deposit tend to be deeper and its basal age tend to be older at the original nucleation sites / center of the peatland complex (Bauer et al., 2003; Mathijssen et al., 2017). As mentioned earlier, field measurements tend to take samples from the deeper part of a peatland complex and shallow peat are underrepresented. The model, however, only simulates peat growth in the vertical dimension and lacks an explicit representation of the lateral development of a peatland in grid-based simulations, thus simulated peat C (per unit peatland area) is diluted when the simulated peatland area fraction in the grid cell increases. In addition, while a dated peat core tells us net burial of peat C during time intervals, the model can't provide a peat age-depth profile because it simulates peat C accumulation based on decomposition of soil C pools, rather than tracking peat C as cohorts over depth/time (Heinemeyer et al., 2010).

The above-noted discrepancies between the simulation and the observation highlight both the need for more peat core data collected with more rigorous sampling methodologies and the need to improve the model. In parallel with this study, ^{14}C dynamics in the soil has been incorporated into the ORCHIDEE-SOM model (Tifafi et al., 2018), which may give us an opportunity to compare simulated ^{14}C age-depth profiles with dated peat C profiles in the future after being merged with our model.

Simulated peatland area development

The initiation and development of peatlands in NA followed the retreat of the ice sheets, as a result of the continuing emergence of new land with the potential to become suitable for peatland formation (Gorham et al., 2007; Halsey et al., 2000). To take glacial extent into account for simulating the Holocene development of peatlands, we use ice sheet reconstructions in NA and Eurasia (Fig. S4, S5). Not surprisingly, when ice cover is considered, the area of peatlands that developed before 8 ka is significantly

decreased, while the area that developed after 6 ka is increased (Fig. 13). We use observed frequency distribution of peat basal age from MacDonald et al. (2006) as a proxy of peatland area change over time, following the assumption proposed by Yu (2011) that peatland area increases linearly with the rate of peat initiation. We grouped the data of MacDonald et al. (2006) into 2000-years bins to compare with simulated peatlands area dynamics (Fig. 13). The inclusion of dynamic ice sheet coverage triggering peat inception clearly improved the model performance in replicating peatland area development during the Holocene, though the peatland area before 8 ka is still overestimated by the model in comparison with the observed frequency distribution of basal ages (Fig. 13). In spite of the difference in peatlands area expansion dynamics between the simulation that considered dynamic ice sheets and the one that did not, the model estimates of present-day total peatland area and carbon stock are generally similar (Fig. S10). Without dynamic ice sheet, the model would predict only 0.1 million km^2 more peatland area and 24 Pg more peat C over the Northern Hemisphere (>30 °N). We are aware of two studies that attempted to account for the presence of ice sheets during the Holocene (Kleinen et al., 2012) and the last Glacial Maximum (Spahni et al., 2013) while simulating peatland C dynamics. Kleinen et al. (2012) modelled C accumulation over the past 8000 years in the peatland areas north of 40 °N using the coupled climate carbon cycle model CLIMBER2-LPJ. A decrease of 10 PgC was found when ice sheet extent at 8 ka BP (from the ICE-5G model) was accounted for. Another peatland modelling study conducted by Spahni et al. (2013) with LPX also prescribed ice sheets and land area from the ICE-5G ice-sheet reconstruction (Peltier, 2004), but influences of ice sheet margin fluctuations on simulated peatland area and C accumulation were not explicitly assessed in their study.

The peatland carbon density criterion for peatland expansion (C_{lim}) is an important factor impacting the simulated Holocene trajectory of peatlands development. Without the limitation of C_{lim}, a larger expansion of northern peatlands would occur before 10 ka (Fig. S11). Such a premature, 'explosive' increase of peatland area would result into the overestimation of C accumulated in the early Holocene in the model. In the meantime, peatland area in regions that only have small C input, i.e. Baffin Island, and

663 northeast Russia, would be overestimated (Fig. S12).

Choice of model parameters

665 For the active, slow and passive peat soil carbon pool, the base decomposition rates

666 are 1.0 a^{-1}, 0.027 a^{-1} and 0.0006 a^{-1} at reference temperature of 30 °C, respectively,

667 meaning that the residence times at 10 °C (no moisture and depth limitation) of these

668 three pools are 4 years, 148 years and 6470 years. In equilibrium / near- equilibrium

669 state, simulated C in the active pool takes up only a small fraction of the total peat C,

670 while generally 40% − 80% of simulated peat C are in the slow C pool and about 20%

671 − 60% are in the passive C pool. Assuming that in a peatland, the active, slow and

672 passive pool account for 3%, 60%, and 37% (median values from the model output of

673 the year 2009) of the total peat C, we can get a mean peat C residence time of 2500

674 years. If depth modifier is considered, the C residence time will vary from 2500 years

675 at the soil surface to 13200 years at the 2.5 m depth. For the record, in previous

676 published large-scale diplotelmic peatland models, at 10 °C, C residence time for the

677 acrotelm (depth = 0.3 m) ranged from 10 to 33 years and ranged from 1000 to 30000

678 years for the catotelm (Kleinen et al., 2012; Spahni et al., 2013; Wania et al., 2009b).

679 We performed sensitivity tests to show the sensitivity of the modelled peat C to model

680 parameters at the 15 northern peatland sites where observed vertical C profiles can be

681 constructed (Table S1). Tested parameters are the e-folding decreasing depth of the

682 depth modifier (z_0, Eq. 2), the prescribed thresholds to start C transfer between soil

683 layers (f_{th}, Eq. 5) and the prescribed fraction of C transferred vertically (f, Eq. 4). We

684 found that changing f_{th} or f leads to only small effects on the vertical soil C profile

685 (see e.g. Burnt Village peat site in Fig. S13). The parameter z_0, by contrast, exerts a

686 relatively strong control over C profiles. It is noteworthy that while our model resolves

687 water diffusion between soil layers according to the Fokker–Planck equation (Qiu et al.,

688 2018), simulated soil moisture does not necessarily increase with depth (Fig. S14). z_0

689 is therefore an important parameter to constrain peat decomposition rates at depth. With

690 smaller z_0, decomposition of C decreases rapidly with depth, resulting in deeper C

691 profile (Fig. S13). Regional scale tests verified these behaviors of the model: When

692 $f_{th} = 0.9$ is used (instead of $f_{th} = 0.7$), changes in peatland area and peat C stock are

693 negligible (Fig. S15). Without z_0, simulated northern peatlands area will not change

694 (3.9 million km2), but northern peatlands C stock will be underestimated (only 300PgC).

695 If $z_0 = 0.5\,\text{m}$ is applied (instead of $z_0 = 1.5\,\text{m}$), the simulated total peat C would

696 triple while the total peatland area would only increase by 0.2 million km^2 (Fig. S16).

697 **Uncertainties in peatland area and soil C estimations**

698 There are large uncertainties in estimates of peatland distribution and C storage.

699 Some studies prescribe peatlands from wetlands. However, in spite of the fact that there

700 are extensive disagreements between wetland maps, it is a challenge to distinguish

701 peatlands from non-peat forming wetlands (Gumbricht et al., 2017; Kleinen et al., 2012;

702 Melton et al., 2013; Xu et al., 2018). Estimates based on peatland inventories are

703 impeded by poor availability of data, non-uniform definitions of peatlands among

704 regions and coarse resolutions (Joosten, 2010; Yu et al., 2010). In addition, as peatlands

705 are normally defined as waterlogged ecosystems with a minimum peat depth of 30 cm

706 or 40 cm, shallow peats are underrepresented. Another approach to estimate peatland

707 area and peat C is to use a soil organic matter map to outline organic-rich areas, such

708 as histosols and histels (Köchy et al., 2015; Spahni et al., 2013). This approach

709 overlooks local hydrological conditions and vegetation composition (Wu et al., 2017).

710 Our model estimates of peatland area and C stock generally fall well within the range

711 of published estimates, except in southeastern US, where there is only 0.05 – 0.10

712 million km^2 of peatland in observations but 0.37 million km^2 in the model prediction

713 (Fig. 7d, Table 3). From early 1600's to 2009, ~ 50% of the original wetlands in the

714 lower 48 states of US have been lost to agricultural, urban development and other

715 development (Dahl, 2011; Tiner Jr, 1984). Although wetlands are not necessarily

716 peatlands, the reported losses of wetlands in US indicating that a potentially large area

717 of peatlands in US may have been lost to land use change. However, historical losses

718 of peatlands due to land use change and the impact of agricultural drainage of peatlands

719 haven't been taken into account by our model. Another factor that might have

720 contributed to the overestimation is a limitation of TOPMODEL, namely that the

721 'floodability' of a pixel in the model is determined by its compound topographic index

722 (CTI) value regardless of the pixel's location along the stream, and thus the floodability

of an upstream pixel with a large CTI might be affected by downstream pixels that have small CTI. The model's inability to resolve small-scale streamflows might be another cause of the overestimation.

The simulated mean annual NPP, HR and NEP of northern peatlands increase from about 1950 onwards. We find positive relationships between NPP and temperature, NPP and atmospheric CO_2 concentration, as well as HR and temperature over the past century (Fig. S9). From a future perspective, it is unclear whether the increasing trend of NEP can be maintained. While photosynthetic sensitivity to CO_2 decreases with increasing atmospheric CO_2 concentration and photosynthesis may finally reach a saturation point in the future, decomposition is not limited by CO_2 concentration and may continue to increase with increasing temperature (Kirschbaum, 1994; Wania et al., 2009b).

Our model applies a multi-layer approach to simulate process-based vertical water fluxes and dynamic C profiles of northern peatlands, highlights the vertical heterogeneities in the peat profile in comparison to previous diplotelmic models (Kleinen et al., 2012; Spahni et al., 2013; Stocker et al., 2014; Wania et al., 2009b). While simulating peatland dynamics, large-scale models used a static peatland distribution map obtained from peat inventories / soil classification map (Largeron et al., 2018; Wania et al., 2009b, 2009a), or prescribed the trajectory of peatland area development over time (Spahni et al., 2013), or used wetland area dynamics as a proxy (Kleinen et al., 2012). We adapt the scheme of DYPTOP to simulate spatial and temporal dynamics of northern peatland area by combing simulated inundation and a set of peatland expansion criteria (Stocker et al., 2014).

As a large-scale LSM which is designed for large-scale gridded applications, ORCHIDEE-PEAT v2.0 cannot explicitly model the lateral development of a peatland. The model therefore aims to simulate average peat depth and C profile in a grid location rather than capturing peat inception time and age-depth profiles of peat cores. For tropical peatlands, the model needs to be improved to represent its tree dominance, oxidation of deeper peat due to pneumatophore (breather roots) of tropical trees, and the greater water table fluctuations as a result of the higher hydraulic conductivity of

753 wood peats and tropical climates (Lawson et al., 2014). In addition, tropical peat is

754 formed as riparian seasonally flooded wetlands with water coming from upstream river

755 networks, whereas the TOPMODEL equations used here implicitly assume a peatland

756 is formed in a grid cell only from rainfall water falling into that grid-cell. Further work

757 to improve this simulation framework is needed in areas such as an accurate

758 representation of the Holocene climate, higher spatial resolution, distinguish bogs from

759 fens to better parameterize water inflows into peatland. Including CH_4 emissions and

760 leaching of DOC will be helpful to get a more complete picture of peatland C budget.

761 **6. Conclusions**

762 Multi-layer schemes have been proven to be superior to simple box configurations in

763 ESMs at realistic modeling of energy, water and carbon fluxes over multilayer

764 ecosystems (De Rosnay et al., 2000; Jenkinson & K. Coleman, 2008; Best et al., 2011;

765 Wu et al., 2016). We apply multi-layer approaches to model vertical profiles of water

766 fluxes and vertical C profiles of northern peatlands. Besides representations of peatland

767 hydrology, peat C decomposition and accumulation, a dynamic model of peatland

768 extent is also included. The model shows good performance at simulating average peat

769 depth and vertical C profile in grid-based simulations. Modern total northern peatlands

770 area and C stock is simulated as 3.9 million km^2 and 463 PgC (Leptosols and

771 agricultural peatlands have been marsked), respectively. While this study investigated

772 the capability of ORCHIDEE-PEAT v2.0 to hindcast the past, in ongoing work, the

773 model is being used to explore how peatlands area and C cycling may change under

774 future climate scenarios.

775

776

777

778

779

780

781

782

783

784

785 Author contribution:

786 CQ implemented peatland water and carbon processes into ORCHIDEE-MICT,
787 introduced the dynamic peatland area module and performed the simulation. DZ
788 contributed to ensuring consistency between the peatland modules and various other
789 processes and modules in the model. PC conceived the project. PC, BG, GK, DZ and
790 CQ contributed to improving the research and interpreting results. SP assisted in
791 implementing of the cost-efficient TOPMODEL. AT and AD provided the dataset of
792 wetland areas. SP, AT, AD and AH contributed to the calibration of the TOPMODEL.
793 All authors contributed to the manuscript.

794

795 Code availability:

796 The source code is available online via:

797 https://forge.ipsl.jussieu.fr/orchidee/wiki/GroupActivities/CodeAvalaibilityPublicatio
798 n/ORCHIDEE_PEAT_V2.

799 Readers interested in running the model should follow the instructions at
800 http://orchidee.ipsl.fr/index.php/you-orchidee.

801

802 Acknowledgements:

803 This study was supported by the European Research Council Synergy grant ERC-2013-
804 SyG-610028 IMBALANCE-P. Adam Hastie received financial support from the
805 European Union's Horizon 2020 research and innovation program under the Marie
806 Sklodowska- Curie grant agreement No. 643052 (C-CASCADES project). We thank
807 Zicheng Yu for providing the peatland distribution map.

808

809 Conflict of Interest: The authors declare no conflict of interest.

References

Alexandrov, G. A., Brovkin, V. A. and Kleinen, T.: The influence of climate on peatland extent in Western Siberia since the Last Glacial Maximum, Sci. Rep., 6, 24784, 2016.

Aurela, M., Riutta, T., Laurila, T., TUOVINEN, J., Vesala, T., TUITTILA, E., Rinne, J., Haapanala, S. and Laine, J.: CO2 exchange of a sedge fen in southern Finland—the impact of a drought period, Tellus B, 59(5), 826–837, 2007.

Batjes, N. H.: Harmonized soil property values for broad-scale modelling (WISE30sec) with estimates of global soil carbon stocks, Geoderma, 269(February), 61–68, doi:10.1016/j.geoderma.2016.01.034, 2016.

Bauer, I. E., Gignac, L. D. and Vitt, D. H.: Development of a peatland complex in boreal western Canada: lateral site expansion and local variability in vegetation succession and long-term peat accumulation, Can. J. Bot., 81(8), 833–847, 2003.

Belyea, L. R. and Clymo, R. S.: Feedback control of the rate of peat formation, Proc. R. Soc. B Biol. Sci., 268(1473), 1315–1321, doi:10.1098/rspb.2001.1665, 2001.

Belyea, L. R. and Malmer, N.: Carbon sequestration in peatland: Patterns and mechanisms of response to climate change, Glob. Chang. Biol., 10(7), 1043–1052, doi:10.1111/j.1365-2486.2004.00783.x, 2004.

Benavides, J. C.: The effect of drainage on organic matter accumulation and plant communities of high-altitude peatlands in the Colombian tropical Andes, Mires Peat, 15, 1–15, 2014.

Best, M. J., Pryor, M., Clark, D. B., Rooney, G. G. and Essery, R. L. H.: The Joint UK Land Environment Simulator (JULES), model description – Part 1 : Energy and water fluxes, Geosci. Model Dev., 4(3), 677–699, doi:10.5194/gmd-4-677-2011, 2011.

Beven, K. J. and Kirkby, M. J.: A physically based, variable contributing area model of basin hydrology bassin versant, Hydrol. Sci. J., 24(1), 43–69, 1979.

Borren, W., Bleuten, W. and Lapshina, E. D.: Holocene peat and carbon accumulation rates in the southern taiga of western Siberia, Quat. Res., 61(1), 42–51, doi:10.1016/j.yqres.2003.09.002, 2004.

Carlson, K. M., Gerber, J. S., Mueller, N. D., Herrero, M., MacDonald, G. K., Brauman, K. A., Havlik, P., O'Connell, C. S., Johnson, J. A., Saatchi, S. and West, P. C.: Greenhouse gas emissions intensity of global croplands, Nat. Clim. Chang., 1(21 November), 1–34, doi:10.1038/nclimate3158, 2016.

Carrara, P. E., Trimble, D. A. and Rubin, M.: Holocene treeline fluctuations in the northern San Juan Mountains, Colorado, USA, as indicated by radiocarbon-dated conifer wood, Arct. Alp. Res., 23(3), 233–246, 1991.

Charmen, D. J.: Blanket mire formation at the Cross Lochs, Sutherland, northern Scotland, Boreas, 21(1), 53–72, doi:10.1111/j.1502-3885.1992.tb00013.x, 1992.

Chaudhary, N., Miller, P. A. and Smith, B.: Modelling Holocene peatland dynamics with an individual-based dynamic vegetation model, Biogeosciences, 14(10), 2571, doi:10.5194/bg-2016-319, 2017a.

Chaudhary, N., Miller, P. A. and Smith, B.: Modelling Holocene peatland dynamics with an individual-based dynamic vegetation model, Biogeosciences, 14(10), 2571, doi:10.5194/bg-2016-319, 2017b.

Chaudhary, N., Miller, P. A. and Smith, B.: Modelling past, present and future peatland

carbon accumulation across the pan-Arctic, Biogeosciences, 14(18), 4023, doi:10.5194/bg-2017-34, 2017c.

Chu, H., Gottgens, J. F., Chen, J., Sun, G., Desai, A. R., Ouyang, Z., Shao, C. and Czajkowski, K.: Climatic variability, hydrologic anomaly, and methane emission can turn productive freshwater marshes into net carbon sources, Glob. Chang. Biol., 21(3), 1165–1181, doi:10.1111/gcb.12760, 2015.

Ciais, P., Sabine, C., Bala, G., Bopp, L., Brovkin, V., Canadell, J., Chhabra, A., DeFries, R., Galloway, J. and Heimann, M.: Carbon and Other Biogeochemical Cycles In Stocker TF, Qin D, Plattner GK, Tignor M, Allen SK, Boschung J, Nauels A, Xia Y, Bex V, Midgley PM eds, Climate Change 2013: The Physical Science Basis. Contribution of Working Group I to the Fifth Assessment Repo, 2013.

Clymo, R. S., Turunen, J. and Tolonen, K.: Carbon Accumulation in Peatland, Oikos, 81(2), 368, doi:10.2307/3547057, 1998.

Cresto Aleina, F., Runkle, B. R. K., Kleinen, T., Kutzbach, L., Schneider, J. and Brovkin, V.: Modeling micro-topographic controls on boreal peatland hydrology and methane fluxes, Biogeosciences, 12(19), 5689–5704, doi:10.5194/bg-12-5689-2015, 2015.

Dahl, T. E.: Status and trends of wetlands in the conterminous United States 2004 to 2009, US Department of the Interior, US Fish and Wildlife Service, Fisheries and …., 2011.

Fan, Y., Li, H. and Miguez-Macho, G.: Global patterns of groundwater table depth, Science (80-.)., 339(6122), 940–943, 2013.

Fan, Z., Neff, J. C., Waldrop, M. P., Ballantyne, A. P. and Turetsky, M. R.: Transport of oxygen in soil pore-water systems: implications for modeling emissions of carbon dioxide and methane from peatlands, Biogeochemistry, 121(3), 455–470, doi:10.1007/s10533-014-0012-0, 2014.

Flanagan, L. B. and Syed, K. H.: Stimulation of both photosynthesis and respiration in response to warmer and drier conditions in a boreal peatland ecosystem, Glob. Chang. Biol., 17(7), 2271–2287, doi:10.1111/j.1365-2486.2010.02378.x, 2011.

Fluet-Chouinard, E., Lehner, B., Rebelo, L.-M., Papa, F. and Hamilton, S. K.: Development of a global inundation map at high spatial resolution from topographic downscaling of coarse-scale remote sensing data, Remote Sens. Environ., 158, 348–361, 2015.

Frolking, S., Roulet, N. T., Tuittila, E., Bubier, J. L., Quillet, A., Talbot, J. and Richard, P. J. H.: A new model of Holocene peatland net primary production, decomposition, water balance, and peat accumulation, Earth Syst. Dyn. Discuss., 1(1), 115–167, doi:10.5194/esdd-1-115-2010, 2010.

Gallego-Sala, A. V., Charman, D. J., Harrison, S. P., Li, G. and Prentice, I. C.: Climate-driven expansion of blanket bogs in Britain during the Holocene, Clim. Past, 12(1), 129–136, doi:10.5194/cp-12-129-2016, 2016.

Gignac, L. D., Halsey, L. A. and Vitt, D. H.: A bioclimatic model for the distribution of Sphagnum-dominated peatlands in North America under present climatic conditions, J. Biogeogr., 27(5), 1139–1151, 2000.

Glaser, P. H., Hansen, B. C. S., Siegel, D. I., Reeve, A. S. and Morin, P. J.: Rates, pathways and drivers for peatland development in the Hudson Bay Lowlands, northern

Ontario, Canada, J. Ecol., 92(6), 1036–1053, doi:10.1111/j.0022-0477.2004.00931.x, 2004a.

Glaser, P. H., Siegel, D. I., Reeve, A. S., Janssens, J. A. N. A. and Janecky, D. R.: Tectonic drivers for vegetation patterning and landscape evolution in the Albany River region of the Hudson Bay, J. Ecol., 92, 1054–1070, 2004b.

Gorham, E.: Northern peatlands: Role in the carbon cycle and probably responses to climate warming, Ecol. Appl., 1(2), 182–195, doi:10.2307/1941811, 1991.

Gorham, E., Lehman, C., Dyke, A., Janssens, J. and Dyke, L.: Temporal and spatial aspects of peatland initiation following deglaciation in North America, Quat. Sci. Rev., 26(3–4), 300–311, doi:10.1016/j.quascirev.2006.08.008, 2007.

Gorham, E., Lehman, C., Dyke, A., Clymo, D. and Janssens, J.: Long-term carbon sequestration in North American peatlands, Quat. Sci. Rev., 58, 77–82, doi:10.1016/j.quascirev.2012.09.018, 2012.

Guimberteau, M., Zhu, D., Maignan, F., Huang, Y., Chao, Y., Dantec-Nédélec, S., Ottlé, C., Jornet-Puig, A., Bastos, A. and Laurent, P.: ORCHIDEE-MICT (v8. 4.1), a land surface model for the high latitudes: model description and validation, Geosci. Model Dev., 11(1), 121, 2018.

Gumbricht, T., Roman-Cuesta, R. M., Verchot, L., Herold, M., Wittmann, F., Householder, E., Herold, N. and Murdiyarso, D.: An expert system model for mapping tropical wetlands and peatlands reveals South America as the largest contributor, Glob. Chang. Biol., 23(9), 3581–3599, doi:10.1111/gcb.13689, 2017.

Halsey, L. A., Vitt, D. H. and Gignac, L. D.: Sphagnum-dominated peatlands in North America since the last glacial maximum: their occurrence and extent, Bryologist, 334–352, 2000.

Heinemeyer, A., Croft, S., Garnett, M. H., Gloor, E., Holden, J., Lomas, M. R. and Ineson, P.: The MILLENNIA peat cohort model: Predicting past, present and future soil carbon budgets and fluxes under changing climates in peatlands, Clim. Res., 45(1), 207–226, doi:10.3354/cr00928, 2010.

Hugelius, G., Tarnocai, C., Broll, G., Canadell, J. G., Kuhry, P. and Swanson, D. K.: The northern circumpolar soil carbon database: Spatially distributed datasets of soil coverage and soil carbon storage in the northern permafrost regions, Earth Syst. Sci. Data, 5(1), 3–13, doi:10.5194/essd-5-3-2013, 2013.

Hughes, A. L. C., Gyllencreutz, R., Lohne, Ø. S., Mangerud, J. and Svendsen, J. I.: The last Eurasian ice sheets - a chronological database and time-slice reconstruction, DATED-1, Boreas, 45(1), 1–45, doi:10.1111/bor.12142, 2016.

Jackson, R. B., Lajtha, K., Crow, S. E., Hugelius, G., Kramer, M. G. and Piñeiro, G.: The Ecology of Soil Carbon: Pools, Vulnerabilities, and Biotic and Abiotic Controls, Annu. Rev. Ecol. Evol. Syst., 48(1), annurev-ecolsys-112414-054234, doi:10.1146/annurev-ecolsys-112414-054234, 2017.

Jafarov, E. and Schaefer, K.: The importance of a surface organic layer in simulating permafrost thermal and carbon dynamics, Cryosphere, 10(1), 465–475, doi:10.5194/tc-10-465-2016, 2016.

Jenkinson, D. S. and K. Coleman: The turnover of organic carbon in subsoils . Part 2 . Modelling carbon turnover, Eur. J. Soil Sci., (April), 400–413, doi:10.1111/j.1365-

2389.2008.01026.x, 2008.

Joosten, H.: The Global Peatland CO2 picture. Peatland status and drainage related emissions in all countries of the world, Wetl. Int. Ede, 2010 [online] Available from: http://scholar.google.com/scholar?hl=en&btnG=Search&q=intitle:The+Global+Peatla nd+CO+2+Picture+Peatland+status+and+drainage+related+emissions+in+all+countri es+of+the+world#0, 2010.

Kirschbaum, M. U. F.: The Sensitivity of C3 Photosynthesis to Increasing CO2 Concentration - a Theoretical-Analysis of Its Dependence on Temperature and Background CO2 Concentration, Plant, Cell Environ., 17(6), 747–754, doi:10.1111/j.1365-3040.1994.tb00167.x, 1994.

Kleinen, T., Brovkin, V. and Schuldt, R. J.: A dynamic model of wetland extent and peat accumulation: Results for the Holocene, Biogeosciences, 9(1), 235–248, doi:10.5194/bg-9-235-2012, 2012.

Köchy, M., Hiederer, R. and Freibauer, A.: Global distribution of soil organic carbon – Part 1 : Masses and frequency distributions of SOC stocks for the tropics , permafrost regions , wetlands , and the world, Soil, 1(1), 351–365, doi:10.5194/soil-1-351-2015, 2015.

Koven, C. D., Ringeval, B., Friedlingstein, P., Ciais, P., Cadule, P., Khvorostyanov, D., Krinner, G. and Tarnocai, C.: Permafrost carbon-climate feedbacks accelerate global warming, Proc. Natl. Acad. Sci., 108(36), 14769–14774, 2011.

Koven, C. D., Riley, W. J., Subin, Z. M., Tang, J. Y., Torn, M. S., Collins, W. D., Bonan, G. B., Lawrence, D. M. and Swenson, S. C.: The effect of vertically resolved soil biogeochemistry and alternate soil C and N models on C dynamics of CLM4, Biogeosciences, 10(11), 7109–7131, doi:10.5194/bg-10-7109-2013, 2013.

Kremenetski, K. V., Velichko, A. A., Borisova, O. K., MacDonald, G. M., Smith, L. C., Frey, K. E. and Orlova, L. A.: Peatlands of the Western Siberian lowlands: Current knowledge on zonation, carbon content and Late Quaternary history, Quat. Sci. Rev., 22(5–7), 703–723, doi:10.1016/S0277-3791(02)00196-8, 2003.

Krinner, G., Viovy, N., de Noblet-Ducoudré, N., Ogée, J., Polcher, J., Friedlingstein, P., Ciais, P., Sitch, S. and Prentice, I. C.: A dynamic global vegetation model for studies of the coupled atmosphere-biosphere system, Global Biogeochem. Cycles, 19(1), 1–33, doi:10.1029/2003GB002199, 2005.

Kuhry, P. and Turunen, J.: The postglacial development of boreal and subarctic peatlands, in Boreal peatland ecosystems, pp. 25–46, Springer., 2006.

Lafleur, P. M., Moore, T. R., Roulet, N. T. and Frolking, S.: Ecosystem respiration in a cool temperate bog depends on peat temperature but not water table, Ecosystems, 8(6), 619–629, doi:10.1007/s10021-003-0131-2, 2005.

Largeron, C., Krinner, G., Ciais, P. and Brutel-Vuilmet, C.: Implementing northern peatlands in a global land surface model: description and evaluation in the ORCHIDEE high-latitude version model (ORC-HL-PEAT), Geosci. Model Dev., 11(8), 3279–3297, 2018.

Lawson, I. T., Jones, T. D., Kelly, T. J., Coronado, E. N. H. and Roucoux, K. H.: The geochemistry of Amazonian peats, Wetlands, 34(5), 905–915, 2014.

Leifeld, J. and Menichetti, L.: The underappreciated potential of peatlands in global

climate change mitigation strategies, Nat. Commun., 9(1), 1071, 2018.

Lewis, C., Albertson, J., Xu, X. and Kiely, G.: Spatial variability of hydraulic conductivity and bulk density along a blanket peatland hillslope, Hydrol. Process., 26(10), 1527–1537, doi:10.1002/hyp.8252, 2012.

Loisel, J., Yu, Z., Beilman, D. W., Camill, P., Alm, J., Amesbury, M. J., Anderson, D., Andersson, S., Bochicchio, C., Barber, K., Belyea, L. R., Bunbury, J., Chambers, F. M., Charman, D. J., De Vleeschouwer, F., Fia kiewicz-Kozie , B., Finkelstein, S. a., Ga ka, M., Garneau, M., Hammarlund, D., Hinchcliffe, W., Holmquist, J., Hughes, P., Jones, M. C., Klein, E. S., Kokfelt, U., Korhola, a., Kuhry, P., Lamarre, a., Lamentowicz, M., Large, D., Lavoie, M., MacDonald, G., Magnan, G., Makila, M., Mallon, G., Mathijssen, P., Mauquoy, D., McCarroll, J., Moore, T. R., Nichols, J., O'Reilly, B., Oksanen, P., Packalen, M., Peteet, D., Richard, P. J., Robinson, S., Ronkainen, T., Rundgren, M., Sannel, a. B. K., Tarnocai, C., Thom, T., Tuittila, E.-S., Turetsky, M., Valiranta, M., van der Linden, M., van Geel, B., van Bellen, S., Vitt, D., Zhao, Y. and Zhou, W.: A database and synthesis of northern peatland soil properties and Holocene carbon and nitrogen accumulation, The Holocene, 24(9), 1028–1042, doi:10.1177/0959683614538073, 2014.

Lund, M., Christensen, T. R., Lindroth, A. and Schubert, P.: Effects of drought conditions on the carbon dioxide dynamics in a temperate peatland, Environ. Res. Lett., 7(4), 45704, 2012.

Macdonald, G. M., Beilman, D. W., Kremenetski, K. V, Sheng, Y., Smith, L. C. and Velichko, A. a: Rapid early development of circumarctic peatlands and atmospheric CH4 and CO2 variations., Science, 314(5797), 285–288, doi:10.1126/science.1131722, 2006.

MacDonald, G. M., Beilman, D. W., Kremenetski, K. V., Sheng, Y., Smith, L. C. and Velichko, A. A.: Rapid Early Development of Circumarctic Peatlands and Atmospheric CH4 and CO2 Variations, Science (80-.)., 314(5797), 285–288, doi:10.1126/science.1131722, 2006.

Madole, R. F.: Bog Stratigraphy, Radiocarbon-Dates, and Pinedale to Holocene Glacial History in Front Range, Colorado, J. Res. Us Geol. Surv., 4(2), 163–169 [online] Available from: isi:A1976BR69000004, 1976.

Marcott, S. a., Shakun, J. D., Clark, P. U. and Mix, A. C.: A Reconstruction of Regional and Global Temperature for the Past 11,300 Years, Science (80-.)., 339(6124), 1198–1201, doi:10.1126/science.1228026, 2013.

Mathijssen, P. J. H., Kähkölä, N., Tuovinen, J. P., Lohila, A., Minkkinen, K., Laurila, T. and Väliranta, M.: Lateral expansion and carbon exchange of a boreal peatland in Finland resulting in 7000 years of positive radiative forcing, J. Geophys. Res. Biogeosciences, 122(3), 562–577, doi:10.1002/2016JG003749, 2017.

McCarter, C. P. R. and Price, J. S.: The hydrology of the Bois-des-Bel bog peatland restoration: 10 years post-restoration, Ecol. Eng., 55, 73–81, doi:10.1016/j.ecoleng.2013.02.003, 2013.

Mcgrath, M. J., Ryder, J., Pinty, B., Otto, J., Naudts, K., Valade, A., Chen, Y., Weedon, J. and Luyssaert, S.: A multi-level canopy radiative transfer scheme for ORCHIDEE (SVN r2566), based on a domain-averaged structure factor, , (November),

doi:10.5194/gmd-2016-280, 2016.

Melton, J. R., Wania, R., Hodson, E. L., Poulter, B., Ringeval, B., Spahni, R., Bohn, T., Avis, C. A., Beerling, D. J. and Chen, G.: Present state of global wetland extent and wetland methane modelling: conclusions from a model intercomparison project (WETCHIMP), Biogeosciences, 10, 753–788, 2013.

Mikaloff Fletcher, S. E., Tans, P. P., Bruhwiler, L. M., Miller, J. B. and Heimann, M.: CH4 sources estimated from atmospheric observations of CH4 and its 13C/12C isotopic ratios: 1. Inverse modeling of source processes, Global Biogeochem. Cycles, 18(4), 2004.

Morris, P. J., Waddington, J. M., Benscoter, B. W. and Turetsky, M. R.: Conceptual frameworks in peatland ecohydrology: looking beyond the two-layered (acrotelm–catotelm) model, Ecohydrology, 4(1), 1–11, 2011.

Moyano, F. E., Vasilyeva, N., Bouckaert, L., Cook, F., Craine, J., Curiel Yuste, J., Don, A., Epron, D., Formanek, P., Franzluebbers, A., Ilstedt, U., Kätterer, T., Orchard, V., Reichstein, M., Rey, A., Ruamps, L., Subke, J. A., Thomsen, I. K. and Chenu, C.: The moisture response of soil heterotrophic respiration: Interaction with soil properties, Biogeosciences, 9(3), 1173–1182, doi:10.5194/bg-9-1173-2012, 2012.

Nachtergaele, F.: The classification of Leptosols in the World Reference Base for Soil Resources, in 19th World Congress of Soil Science, Soil Solutions for a Changing World, pp. 1–6., 2010.

Oleszczuk, R. and Truba, M.: The analysis of some physical properties of drained peat-moorsh soil Layers, Ann. Warsaw Univ. Life Sci. L. Reclam., 45(1), 41–48, 2013.

Packalen, M. S., Finkelstein, S. A. and McLaughlin, J. W.: Carbon storage and potential methane production in the Hudson Bay Lowlands since mid-Holocene peat initiation, Nat. Commun., 5(July 2015), 4078, doi:10.1038/ncomms5078, 2014.

Packalen, M. S., Finkelstein, S. A. and McLaughlin, J. W.: Climate and peat type in relation to spatial variation of the peatland carbon mass in the Hudson Bay Lowlands, Canada, J. Geophys. Res. G Biogeosciences, 121(4), 1104–1117, doi:10.1002/2015JG002938, 2016.

Parish, F., Sirin, A., Charman, D., Joosten, H., Minayeva, T., Silvius, M. and Stringer, L.: Assessment on Peatlands, Biodiversity and Climate Change: Main Report., 2008.

Parmentier, F. J. W., van der Molen, M. K., de Jeu, R. A. M., Hendriks, D. M. D. and Dolman, A. J.: CO2 fluxes and evaporation on a peatland in the Netherlands appear not affected by water table fluctuations, Agric. For. Meteorol., 149(6–7), 1201–1208, doi:10.1016/j.agrformet.2008.11.007, 2009.

Peltier, W. R.: Global glacial isostasy and the surface of the ice-age Earth: the ICE-5G (VM2) model and GRACE, Annu. Rev. Earth Planet. Sci., 32, 111–149, 2004.

Portmann, F. T., Siebert, S. and Döll, P.: MIRCA2000-Global monthly irrigated and rainfed crop areas around the year 2000: A new high-resolution data set for agricultural and hydrological modeling, Global Biogeochem. Cycles, 24(1), doi:10.1029/2008GB003435, 2010.

Price, J. S., Cagampan, J. and Kellner, E.: Assessment of peat compressibility: Is there an easy way?, Hydrol. Process., 19(17), 3469–3475, doi:10.1002/hyp.6068, 2005.

Prigent, C., Papa, F., Aires, F., Rossow, W. B. and Matthews, E.: Global inundation

dynamics inferred from multiple satellite observations, 1993-2000, J. Geophys. Res. Atmos., 112(12), 1–13, doi:10.1029/2006JD007847, 2007.

Prigent, C., Papa, F., Aires, F., Jimenez, C., Rossow, W. B. and Matthews, E.: Changes in land surface water dynamics since the 1990s and relation to population pressure, Geophys. Res. Lett., 39(8), 2–6, doi:10.1029/2012GL051276, 2012.

Qiu, C., Zhu, D., Ciais, P., Guenet, B., Krinner, G., Peng, S., Aurela, M., Bernhofer, C., Brümmer, C., Bret-Harte, S., Chu, H., Chen, J., Desai, A. R., Dušek, J., Euskirchen, E. S., Fortuniak, K., Flanagan, L. B., Friborg, T., Grygoruk, M., Gogo, S., Grünwald, T., Hansen, B. U., Holl, D., Humphreys, E., Hurkuck, M., Kiely, G., Klatt, J., Kutzbach, L., Largeron, C., Laggoun-Défarge, F., Lund, M., Lafleur, P. M., Li, X., Mammarella, I., Merbold, L., Nilsson, M. B., Olejnik, J., Ottosson-Löfvenius, M., Oechel, W., Parmentier, F.-J. W., Peichl, M., Pirk, N., Peltola, O., Pawlak, W., Rasse, D., Rinne, J., Shaver, G., Schmid, H. P., Sottocornola, M., Steinbrecher, R., Sachs, T., Urbaniak, M., Zona, D. and Ziemblinska, K.: ORCHIDEE-PEAT (revision 4596), a model for northern peatland CO2, water, and energy fluxes on daily to annual scales, Geosci. Model Dev., 11(2), 497–519, doi:10.5194/gmd-11-497-2018, 2018.

Ringeval, B., Decharme, B., Piao, S. L., Ciais, P., Papa, F., De Noblet-Ducoudré, N., Prigent, C., Friedlingstein, P., Gouttevin, I., Koven, C. and Ducharne, A.: Modelling sub-grid wetland in the ORCHIDEE global land surface model: Evaluation against river discharges and remotely sensed data, Geosci. Model Dev., 5(4), 941–962, doi:10.5194/gmd-5-941-2012, 2012.

De Rosnay, P., Bruen, M. and Polcher, J.: Sensitivity of surface fluxes to the number of layers in the soil model used in GCMs, Geophys. Res. Lett., 27(20), 3329–3332, doi:10.1029/2000GL011574, 2000.

Roulet, N. T., Lafleur, P. M., Richard, P. J. H., Moore, T. R., Humphreys, E. R. and Bubier, J.: Contemporary carbon balance and late Holocene carbon accumulation in a northern peatland, Glob. Chang. Biol., 13(2), 397–411, doi:10.1111/j.1365-2486.2006.01292.x, 2007.

Seppälä, M.: Palsa mires in Finland, finnish Environ., 23, 155–162, 2006.

Sitch, S., Smith, B., Prentice, I. C., Arneth, a., Bondeau, a., Cramer, W., Kaplan, J. O., Levis, S., Lucht, W., Sykes, M. T., Thonicke, K. and Venevsky, S.: Evaluation of ecosystem dynamics, plant geography and terrestrial carbon cycling in the LPJ dynamic global vegetation model , Glob. Chang. Biol., 9(2), 161–185, doi:10.1046/j.1365-2486.2003.00569.x, 2003.

Smith, L. C.: Siberian Peatlands a Net Carbon Sink and Global Methane Source Since the Early Holocene, Science (80-.)., 303(2004), 353–356, doi:10.1126/science.1090553, 2004.

Spahni, R., Joos, F., Stocker, B. D., Steinacher, M. and Yu, Z. C.: Transient simulations of the carbon and nitrogen dynamics in northern peatlands: From the Last Glacial Maximum to the 21st century, Clim. Past, 9(3), 1287–1308, doi:10.5194/cp-9-1287-2013, 2013.

Stocker, B. D., Spahni, R. and Joos, F.: DYPTOP: A cost-efficient TOPMODEL implementation to simulate sub-grid spatio-temporal dynamics of global wetlands and peatlands, Geosci. Model Dev., 7(6), 3089–3110, doi:10.5194/gmd-7-3089-2014, 2014.

Sulman, B. N., Desai, a. R., Cook, B. D., Saliendra, N. and Mackay, D. S.: Contrasting carbon dioxide fluxes between a drying shrub wetland in Northern Wisconsin, USA, and nearby forests, Biogeosciences, 6(6), 1115–1126, doi:10.5194/bg-6-1115-2009, 2009.

Tfaily, M. M., Cooper, W. T., Kostka, J. E., Chanton, P. R., Schadt, C. W., Hanson, P. J., Iversen, C. M. and Chanton, J. P.: Organic matter transformation in the peat column at Marcell Experimental Forest: humification and vertical stratification, J. Geophys. Res. Biogeosciences, 119(4), 661–675, 2014.

Tifafi, M., Camino-Serrano, M., Hatté, C., Morras, H., Moretti, L., Barbaro, S., Cornu, S. and Guenet, B.: The use of radiocarbon 14C to constrain carbon dynamics in the soil module of the land surface model ORCHIDEE (SVN r5165), Geosci. Model Dev., 11(12), 4711–4726, doi:10.5194/gmd-11-4711-2018, 2018.

Tiner Jr, R. W.: Wetlands of the United States: current status and recent trends, United States Fish and Wildlife Service., 1984.

Tootchi, A., Jost, A. and Ducharne, A.: Multi-source global wetland maps combining surface water imagery and groundwater constraints, Earth Syst. Sci. Data, 11(1), 189–220, doi:10.5194/essd-11-189-2019, 2019.

Turunen, J., Tahvanainen, T., Tolonen, K. and Pitk??nen, A.: Carbon accumulation in West Siberian mires, Russia, Global Biogeochem. Cycles, 15(2), 285–296, doi:10.1029/2000GB001312, 2001.

Turunen, J., Tomppo, E., Tolonen, K. and Reinikainen, A.: Estimating carbon accumulation rates of undrained mires in Finland – application to boreal and subarctic regions, The Holocene, 12(1), 69–80, doi:10.1191/0959683602hl522rp, 2002.

Wania, R., Ross, I. and Prentice, I. C.: Integrating peatlands and permafrost into a dynamic global vegetation model: 1. Evaluation and sensitivity of physical land surface processes, Global Biogeochem. Cycles, 23(3), 1–19, doi:10.1029/2008GB003412, 2009a.

Wania, R., Ross, I. and Prentice, I. C.: Integrating peatlands and permafrost into a dynamic global vegetation model: 2. Evaluation and sensitivity of vegetation and carbon cycle processes, Global Biogeochem. Cycles, 23(3), 1–15, doi:10.1029/2008GB003413, 2009b.

Wu, Y., Verseghy, D. L. and Melton, J. R.: Integrating peatlands into the coupled Canadian Land Surface Scheme (CLASS) v3.6 and the Canadian Terrestrial Ecosystem Model (CTEM) v2.0, Geosci. Model Dev., 9(8), 2639–2663, doi:10.5194/gmd-9-2639-2016, 2016.

Wu, Y., Chan, E., Melton, J. R. and Verseghy, D. L.: A map of global peatland distribution created using machine learning for use in terrestrial ecosystem and earth system models, Geosci. Model Dev. Discuss., (July), 2017.

Xu, J., Morris, P. J., Liu, J. and Holden, J.: PEATMAP: Refining estimates of global peatland distribution based on a meta-analysis, Catena, 160(September 2017), 134–140, doi:10.1016/j.catena.2017.09.010, 2018.

Yu, Z.: Holocene carbon flux histories of the world's peatlands: Global carbon-cycle implications, The Holocene, 21(5), 761–774, doi:10.1177/0959683610386982, 2011.

Yu, Z., Campbell, I. D., Campbell, C., Vitt, D. H., Bond, G. C. and Apps, M. J.: Carbon

sequestration in western Canadian peat highly sensitive to Holocene wet-dry climate cycles at millennial timescales, The Holocene, 13(6), 801–808, doi:10.1191/0959683603hl667ft, 2003a.

Yu, Z., Vitt, D. H., Campbell, I. D. and Apps, M. J.: Understanding Holocene peat accumulation pattern of continental fens in western Canada, Can. J. Bot., 81(3), 267–282, 2003b.

Yu, Z., Beilman, D. W. and Jones, M. C.: Sensitivity of Northern Peatland Carbon Dynamics to Holocene Climate Change, Carbon Cycl. North. Peatlands, 184, 55–69, doi:10.1029/2008GM000822, 2009.

Yu, Z., Loisel, J., Brosseau, D. P., Beilman, D. W. and Hunt, S. J.: Global peatland dynamics since the Last Glacial Maximum, Geophys. Res. Lett., 37(13), 1–5, doi:10.1029/2010GL043584, 2010.

Yu, Z. C.: Northern peatland carbon stocks and dynamics: A review, Biogeosciences, 9(10), 4071–4085, doi:10.5194/bg-9-4071-2012, 2012.

Zaccone, C., Sanei, H., Outridge, P. M. and Miano, T. M.: Studying the humification degree and evolution of peat down a Holocene bog profile (Inuvik, NW Canada): A petrological and chemical perspective, Org. Geochem., 42(4), 399–408, doi:10.1016/j.orggeochem.2011.02.004, 2011.

Zhang, Z., Zimmermann, N. E., Kaplan, J. O. and Poulter, B.: Modeling spatiotemporal dynamics of global wetlands: Comprehensive evaluation of a new sub-grid TOPMODEL parameterization and uncertainties, Biogeosciences, 13(5), 1387–1408, doi:10.5194/bg-13-1387-2016, 2016.

Zhu, D., Peng, S. S., Ciais, P., Viovy, N., Druel, A., Kageyama, M., Krinner, G., Peylin, P., Ottlé, C., Piao, S. L., Poulter, B., Schepaschenko, D. and Shvidenko, A.: Improving the dynamics of Northern Hemisphere high-latitude vegetation in the ORCHIDEE ecosystem model, Geosci. Model Dev., 8(7), 2263–2283, doi:10.5194/gmd-8-2263-2015, 2015.

1207 **Table 1.** Parameter values in peatland modules of ORCHIDEE-PEAT v2.0.

1208

1209

Parameter	Value	Description
$k_{0,i}$		the base decomposition rate of carbon pools, Eq. 1
$k_{0,i}$: $i{=}active$	1.0 a^{-1}	the base decomposition rate of the active pool at 30 °C, Eq. 1
$k_{0,i}$: $i{=}slow$	0.027 a^{-1}	the base decomposition rate of the slow pool at 30 °C, Eq. 1
$k_{0,i}$: $i{=}passive$	0.0006 a^{-1}	the base decomposition rate of the passive pool at 30 °C, Eq. 1
z_0	1.5m	The e-folding depth of base decomposition rate, Eq. 2
f	0.1	The fraction of carbon content in the model layer to be transported to the layer below, Eq. 4
f_{th}	0.7	The amount (fractional) of carbon content that the model layer need to hold before transporting carbon to the layer below, Eq. 5
m	gridcell specific	TOPMODEL parameter (the saturated hydraulic conductivity decay factor with depth), Fig.1, TextS4
CTI_{min}	gridcell specific	TOPMODEL parameter (the minimum CTI for floodability), Fig.1, TextS4
Num	gridcell specific	The total number of growing season months in the preceding 30 years, Fig.1, Sect. 2.2.2
SWB	6 cm	Minimum summer water balance, Fig.1, Sect. 2.2.2
C_{lim}	50.3 kg C m^{-2}	Minimum peat C density , Fig.1, Sect. 2.2.2

1210

1211

1212

1213

1214

1215

1216

1217

1218

1219
1220
Table 2. Measured and simulated minimum, maximum and median depth (m) of peat cores, grouped by peatland types, ages, and climatic regions. The root mean square errors between observations and simulations are also listed.

1224

	Measured			Simulated			
	Minimum	Maximum	Median	Minimum	Maximum	Median	RMSE
Fens	1.10	7.25	3.78	0.75	4.30	2.16	2.08
Bogs	0.96	10.95	3.30	0.75	5.49	2.18	2.59
Others	1.00	3.95	1.94	0.37	6.64	2.38	2.46
$12\ \text{ka} \leq \text{Age}$	2.45	8.61	3.52	0.37	3.21	2.64	2.78
$10 \leq \text{Age} < 12\ \text{ka}$	1.28	7.24	3.60	1.50	5.40	3.20	2.72
$8 \leq \text{Age} < 10\ \text{ka}$	1.89	10.95	3.25	0.75	6.64	2.16	3.33
$6 \leq \text{Age} < 8\ \text{ka}$	0.96	4.82	3.00	0.75	5.49	2.15	1.54
$4 \leq \text{Age} < 6\ \text{ka}$	1.00	5.75	2.44	0.75	2.18	1.54	1.73
Arctic	1.00	5.10	1.80	0.97	5.48	3.39	2.25
Boreal	0.96	10.95	3.22	0.37	6.64	2.15	2.35
Temperate	3.09	7.24	6.17	1.50	3.20	2.18	3.98
All	0.96	10.95	3.10	0.37	6.64	2.18	2.45

1225

1226

1227

1228

1229

Table 3. Observed (estimates from peatland inventories and soil database) and simulated northern peatland area, countries are sorted in descending order according to the estimate of IMCG-GPD.

country/area	Peatland area (10^3 km^2)			
	IMCG-GPD	WISE	PEATMAP	Simulated $f_{noLEP-CR}$
>30°N	>3000	2823	3250	3896
Russia-Asian part	1176	852	1217	1336
Canada	1134	1031	1095	1009
Russia-European part	199	285	207	392
USA(Alaska)	132	167	72	168
USA(lower 48)	92	49	98	365
Finland	79	89	69	42
Sweden	66	65	58	35
Norway	30	19	14	29
Mongolia	26	13	13	6
Belarus	22	29	22	11
United Kingdom	17	21	17	42
Germany	17	14	13	33
Poland	12	18	16	8
Ireland	11	9	14	17

1244

1245

1246

1247

Table 4. Observed and simulated northern peatland C, countries are sorted
in descending order according to the estimate of IMCG-GPD.

1250

country/area	Peat carbon stock (Pg C)		
	IMCG-GPD	WISE	Simulated $f_{\text{noLEP-CR}}$
>30°N		421	463
Canada	155	155	87
Russia-Asian part	118	114	174
Russia-European part	20	38	49
USA(Alaska)	16	28	32
USA(lower 48)	14	10	45
Finland	5	15	5
Sweden	5	10	4
Norway	2	3	3
Germany	2	3	5
United Kingdom	2	4	7
Belarus	1	4	1
Ireland	1	2	4

1251

1252
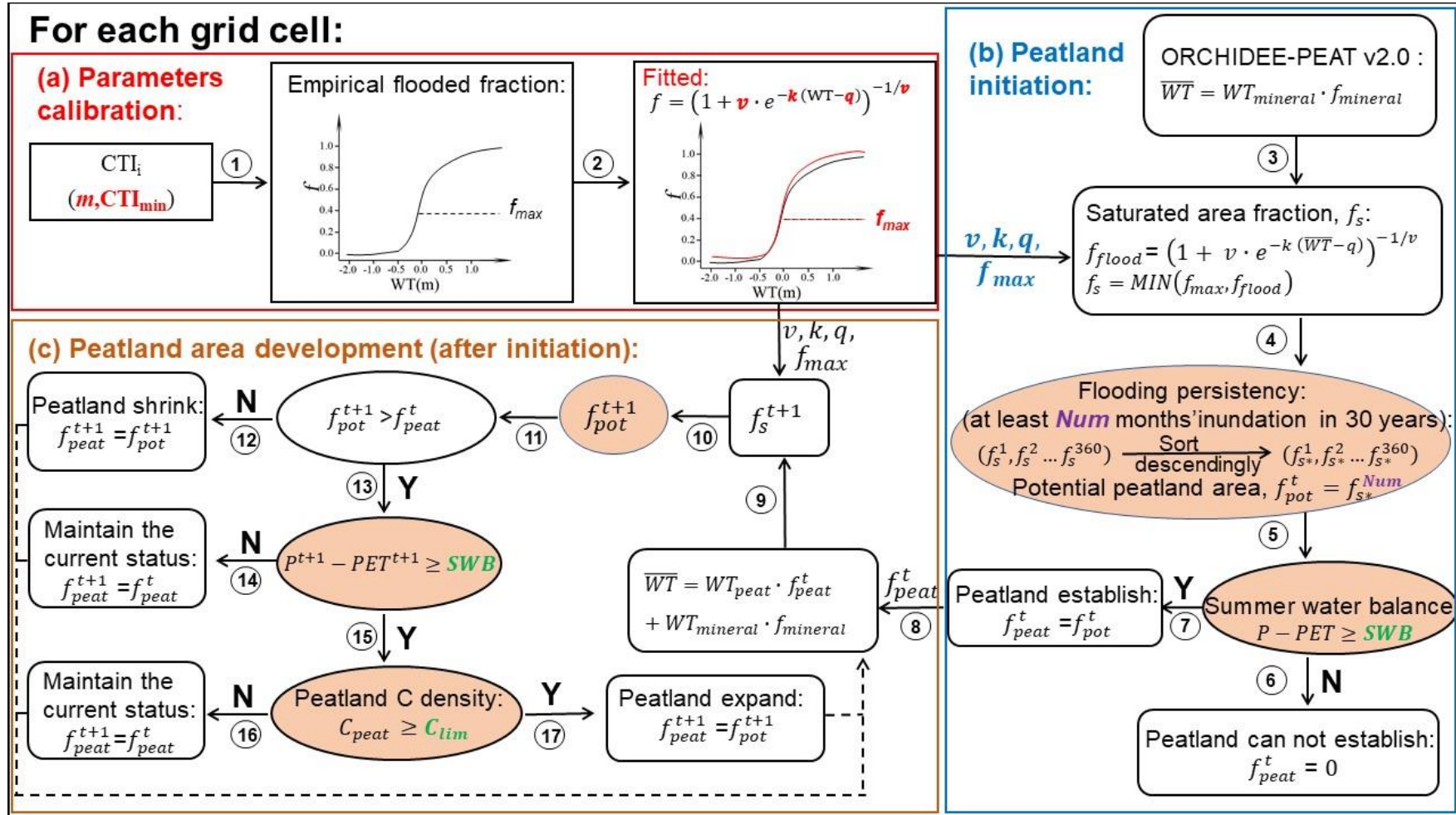
Fig. 1. Information flow of dynamic peatland area module in ORCHIDEE-PEAT v2.0. *Num* is a gridcell-specific parameter, *SWB* and *C_{lim}* are globally uniform parameters (Sect. 2.2)
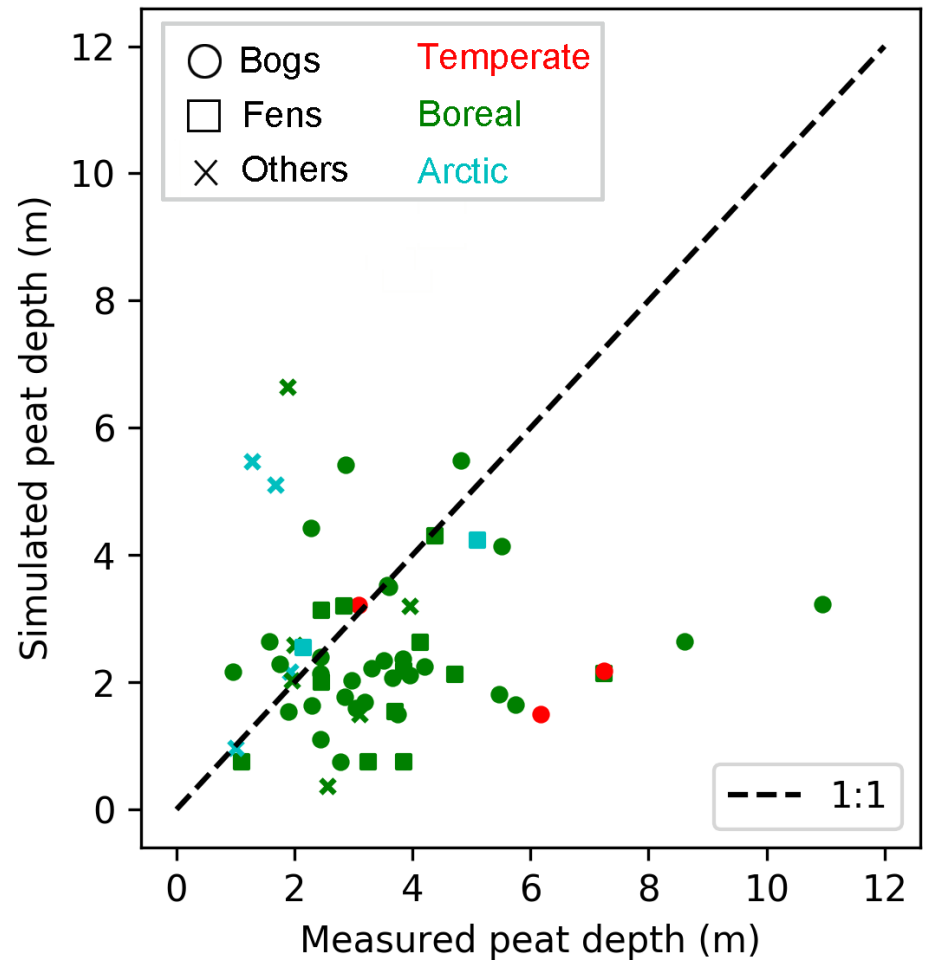
1261 **Fig. 2.** Measured and simulated peat depth at 60 peatlands sites (Table S1). Shapes of
1262 markers indicate peatland types (bogs, fens, others), colors of markers imply climatic
1263 zones (temperate, boreal, arctic) of sites' location.
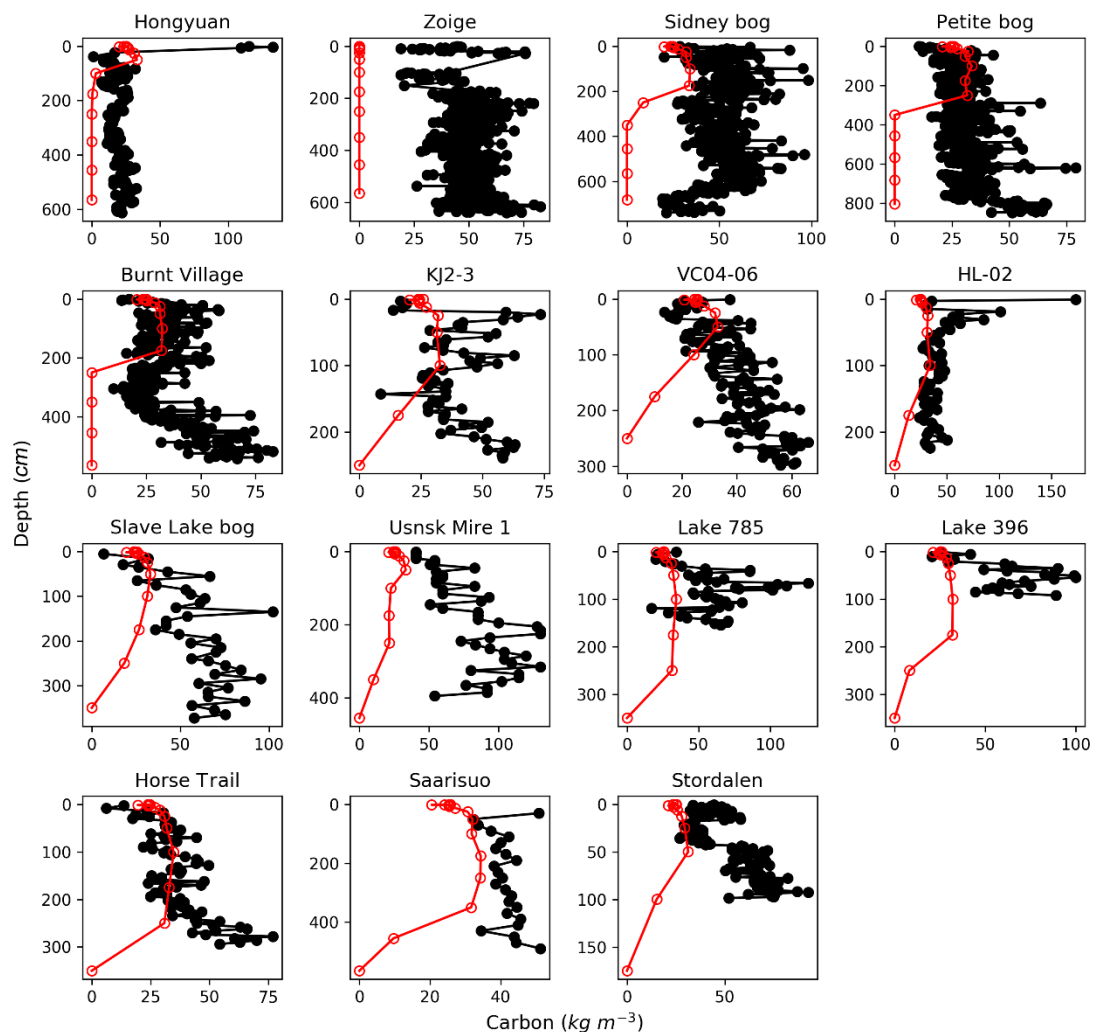
1270 **Fig. 3.** Observed (black) and simulated (red) vertical profiles of soil C, at the 15 sites
1271 where peat age, depth, bulk density and carbon fraction have been measured (Table S1).
1272 The black circles indicate depths of measurements, the red circles indicate the depth of
1273 each soil layer in the model.

1274
1275
1276
1277

1278
1279
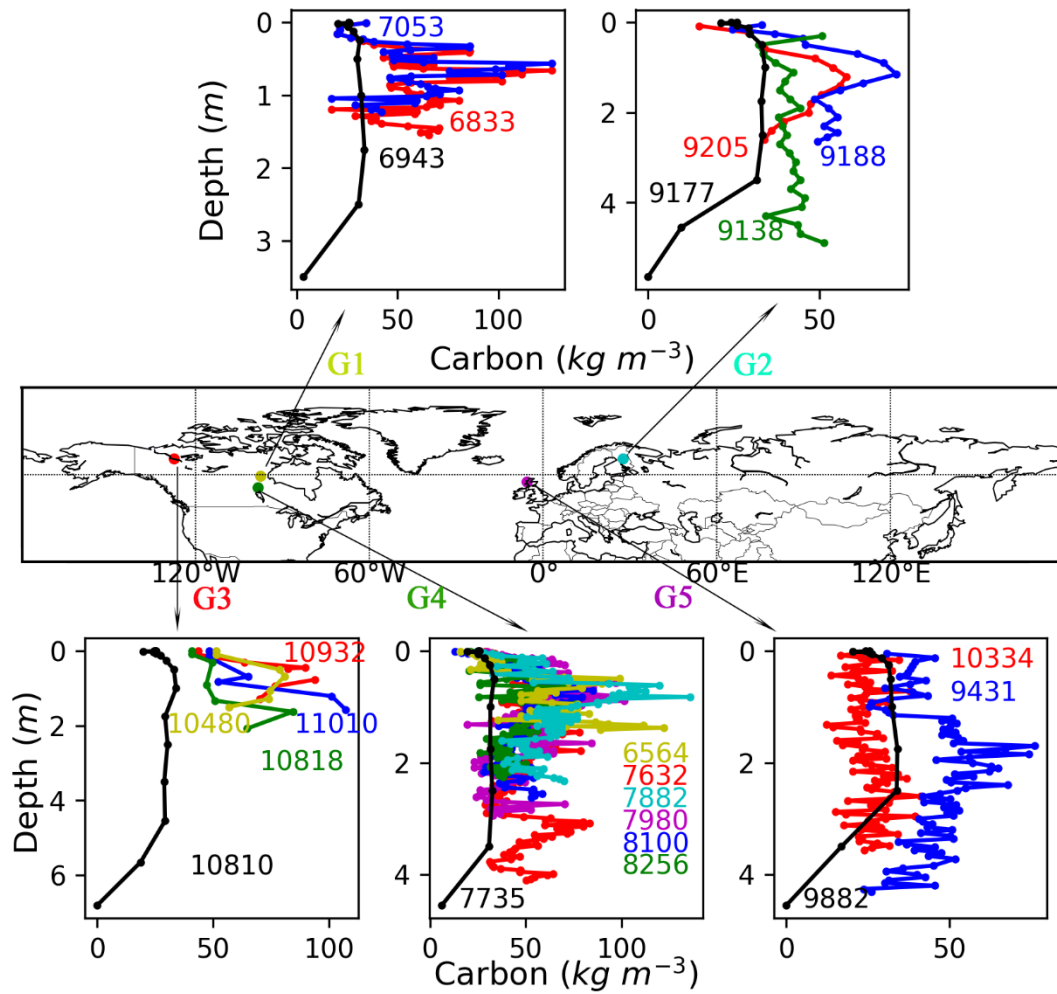
1280
1281

Fig. 4. Observed (colored, with each colored line represent one peat core) and simulated (black) vertical C profiles of five grid cells where there is more than one core. The numbers in the figure indicate ages of sampled peat cores (colored) and time length of the simulation (black, is the mean age of all cores in the same grid cell).

1286
1287
1288
1289

1290
1291
1292
1293
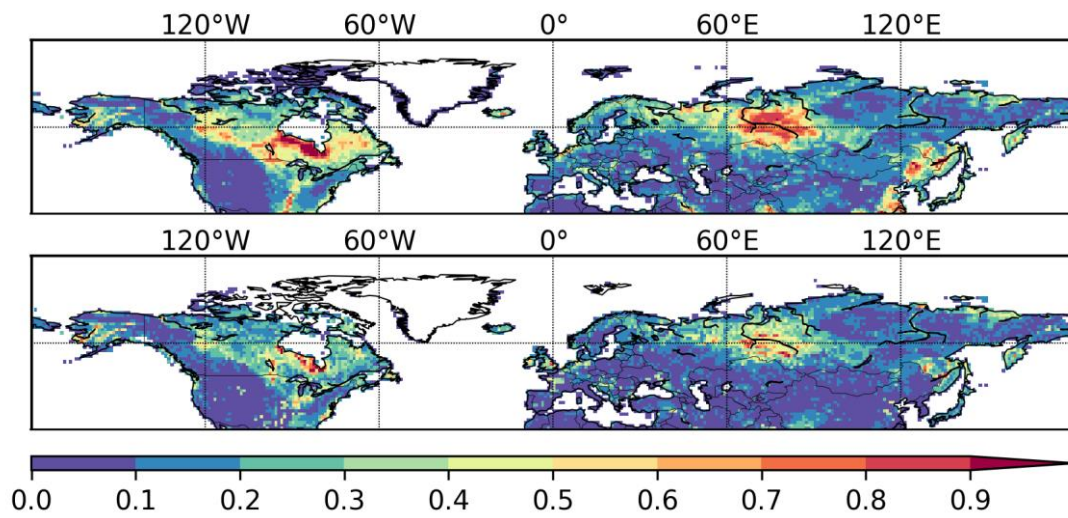
1294
1295
Fig. 5. Wetland area fraction from CW-WTD (upper panel), simulated maximum
inundation areas (lower panel)
1298
1299

1300

1301

1302
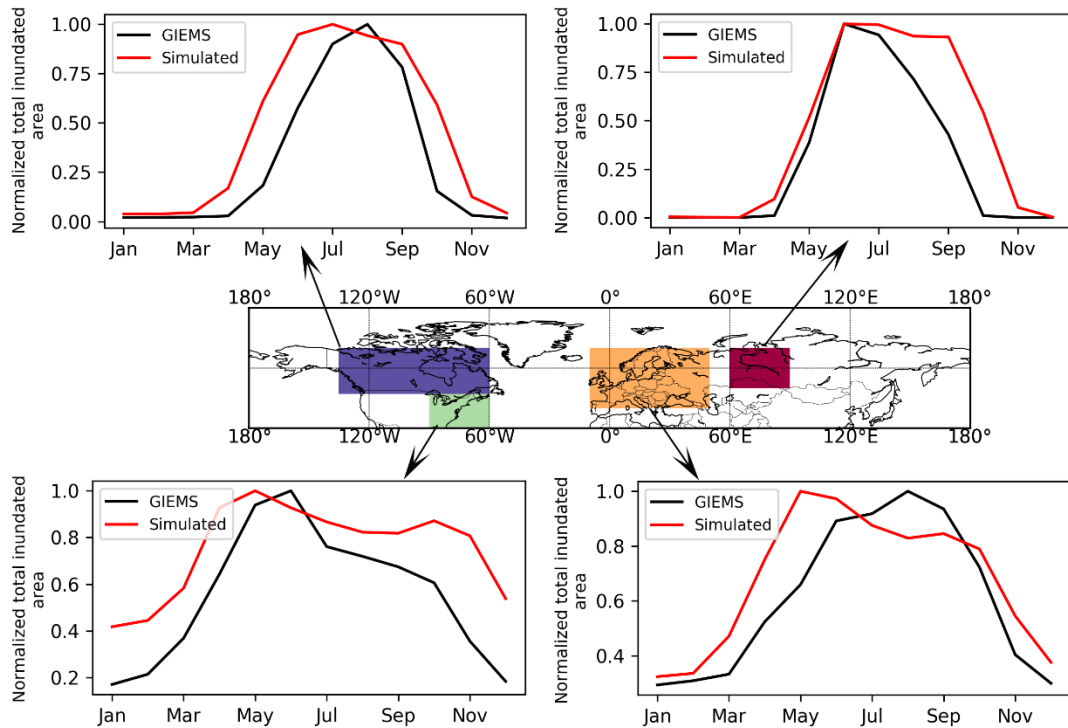
1303

1304 **Fig. 6.** Simulated and observed (GIEMS, (Prigent et al., 2007, 2012)) mean seasonality
1305 (averaged over 1993–2007) of total inundated area. Note that the simulated and
1306 observed total inundated area of each month is divided by the simulated and observed
1307 maximum monthly value, respectively, to highlight seasonality of inundation rather
1308 than comparing absolute values of inundated area.
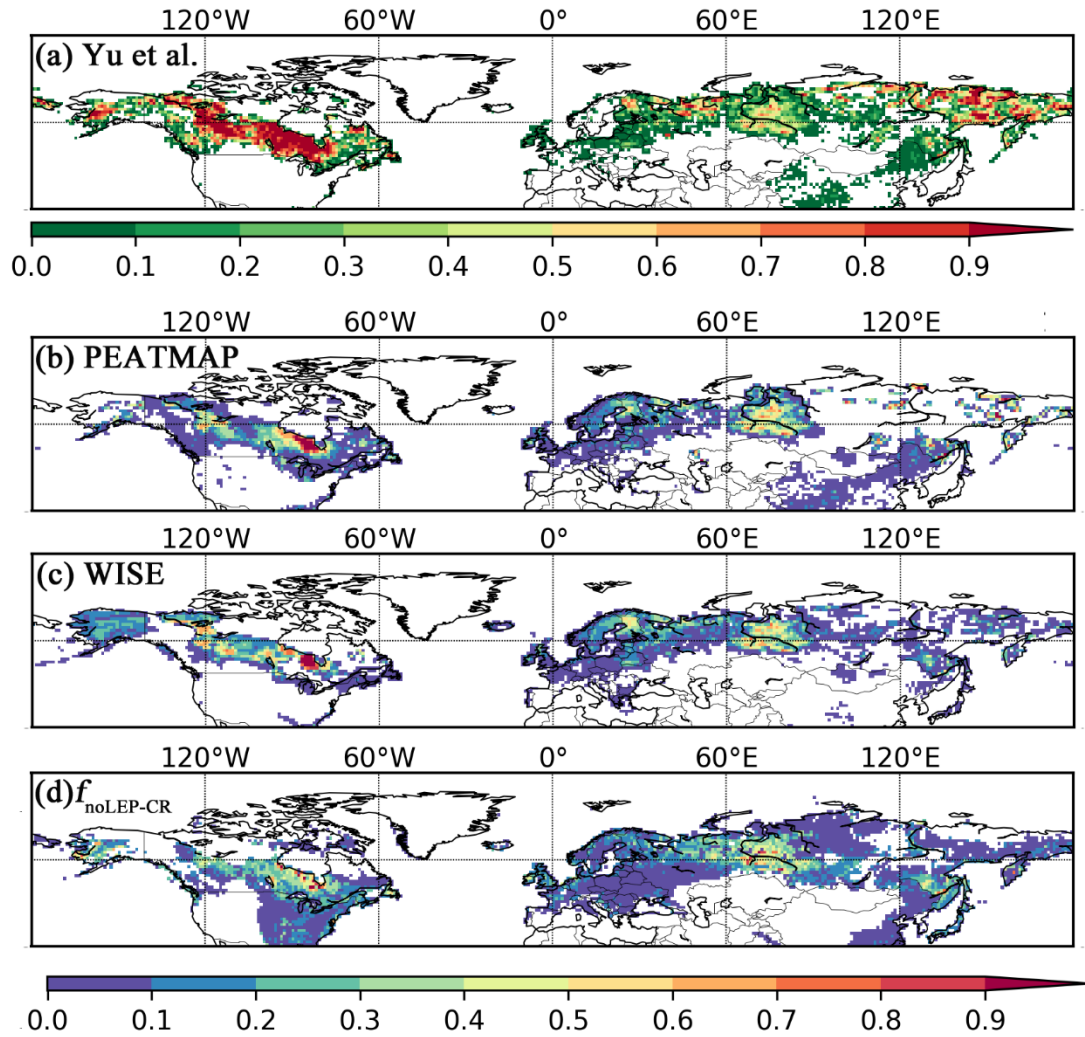
Fig. 7. Observed and simulated peatland area fraction. (a) Peatland fractions obtained from qualitative map of Yu et al. (2010). The original qualitative map only delineates areas with peatland coverage greater than 5%, the quantitively data here is derived by aggregating the interpolated $0.05° \times 0.05°$ grid cells into $1° \times 1°$ fractions, thus it's not directly comparable to the fractional peatland area of other datasets and the model output. We illustrate it with a distinct color key, (b) peatland area fraction derived from the PEATMAP, (c) histosol fractions from the WISE soil database, (d) simulated peatland area fraction ($f_{noLEP-CR}$), with pattern and timing of deglaciation has been considered. Areas dominated by Leptosols has been masked and areas occupied by crops has been excluded, under the assumption that cropland occupied peatland in proportion to grid cell peat fraction.

1328
1329
1330

1331

1332
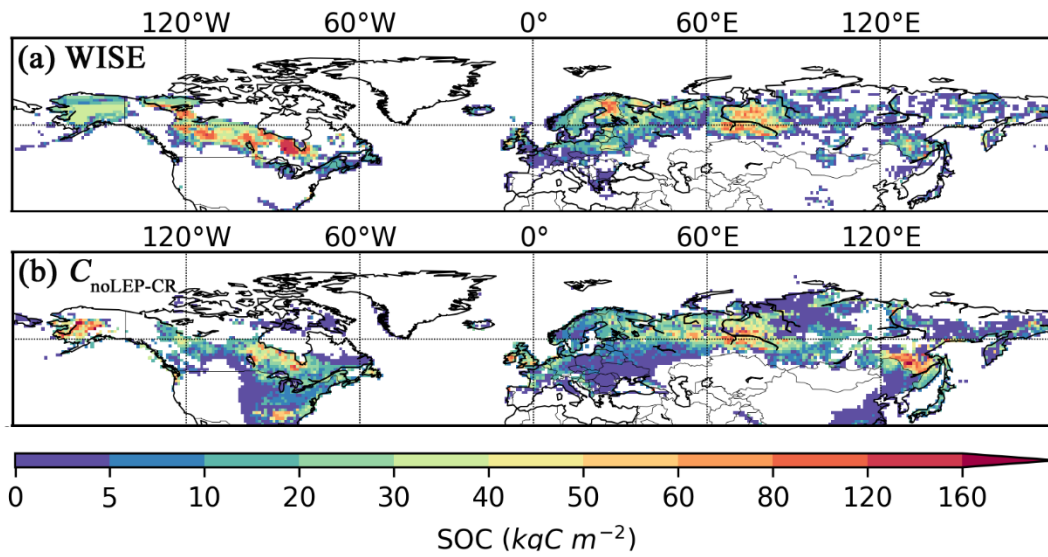
Fig. 8. Observed and simulated peatland soil carbon density. (a) Peatland (Histosols) soil carbon density from the WISE soil database, (b) simulated peatland soil carbon density ($C_{\text{noLEP-CR}}$), with pattern and timing of deglaciation has been considered. Areas dominated by Leptosols has been masked and areas occupied by crops has been excluded, under the assumption that cropland occupied peatland in proportion to grid cell peat fraction.

1339
1340
1341

1342
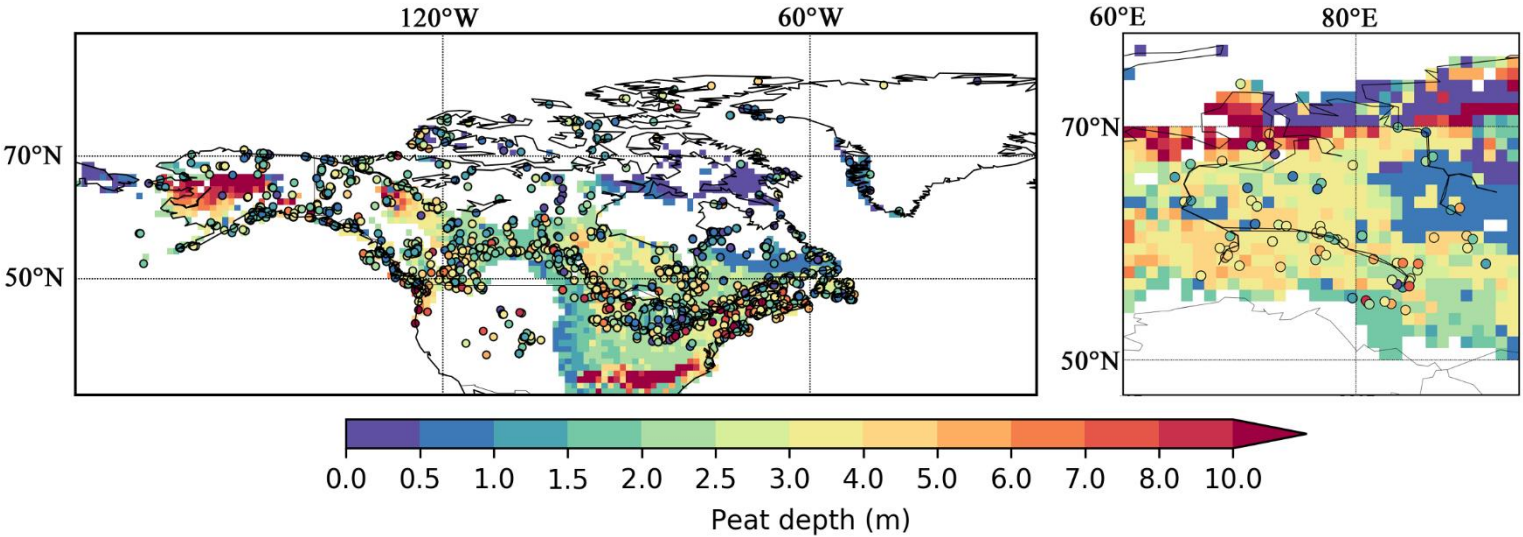
1343
1344
1345 **Fig. 9.** Measured (color filled circles, with colors indicating measured values) and simulated (background maps) peat depth in North America (left)
1346 and in the West Siberian lowlands (right). Measured peat cores from North America are from Gorham et al. (2012), while that from the West
1347 Siberian lowlands are from Kremenetski et al. (2003).
1348

1349

1350

1351

1352
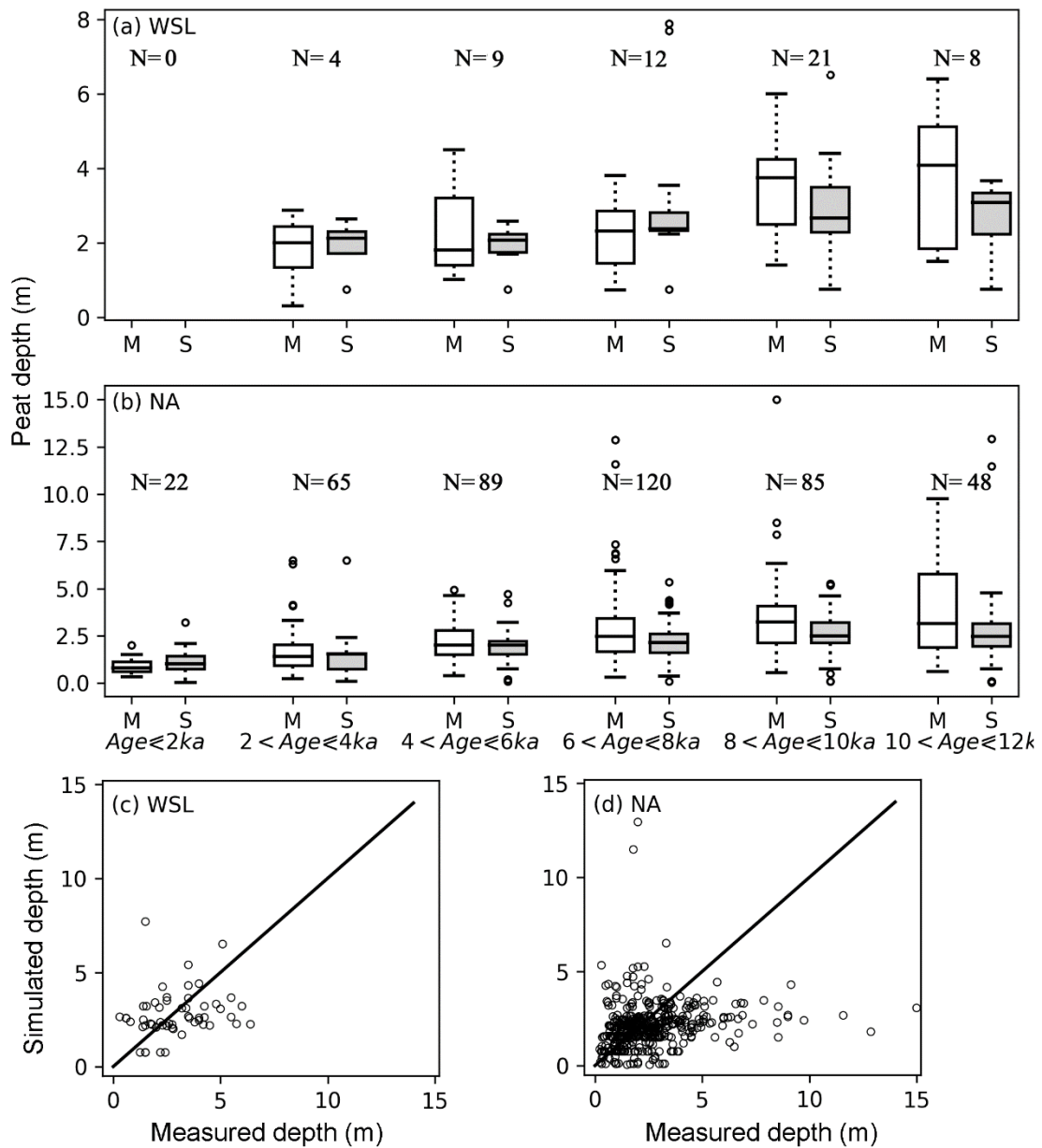
Fig. 10. (a, b) Measured (M) and simulated (S) mean peat depth at the West Siberian lowlands (a) and North America (b), grouped according to the mean age of peat cores. Measured peat cores are from Gorham et al. (2012) and Kremenetski et al. (2003). The horizontal box lines: the upper line - the 75th percentile, the central line - the median (50th percentile), the lower line - the 25th percentile. The dashed lines represent 1.5 times the IQR. The circles are outliers. Number of included grid cells in each age group is indicated by N. (c, d) The scatter plot of measured and simulated peat depth for the West Siberian lowlands (c) and North America (d). For a grid cell that has multiple measured peat cores, the median depth of all measurements is plotted against the simulated depth in the scatter plot.

1353
1354
1355
1356
1357
1358
1359
1360
1361
1362
1363

1364
1365
1366
1367
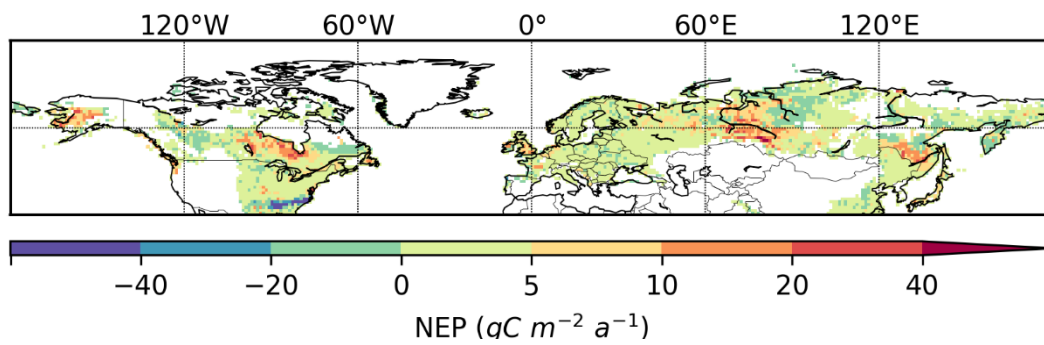
1368
1369
1370 **Fig. 11.** Simulated annual net ecosystem production (NEP), averaged over 1901 – 2009.
1371 Obtained by multiplying peatland NEP (gC m^{-2} peatland a^{-1}) with peatland fraction for
1372 each grid cell.
1373
1374
1375
1376

1377
1378
1379
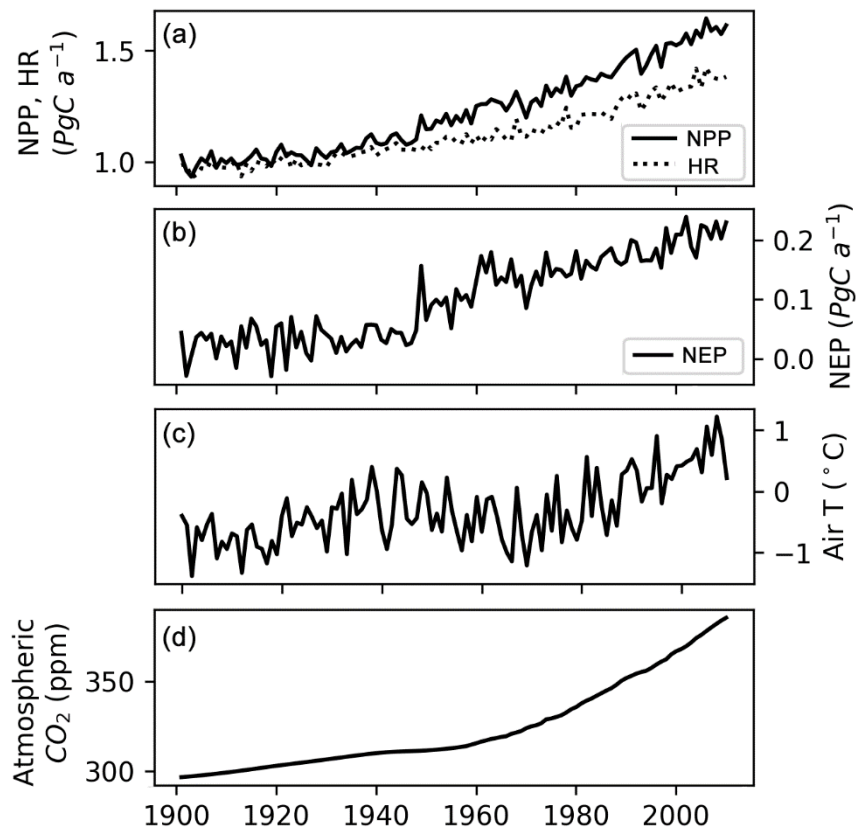
1380
1381
1382 **Fig. 12.** (a) Simulated annual net primary production (NPP), heterotrophic respiration
1383 (HR) of northern peatlands, (b) simulated net ecosystem production (NEP) of northern
1384 peatlands, (c) mean air temperature (T) of grid cells that have peatland, (d) atmospheric
1385 CO_2 concentration.
1386
1387
1388
1389

1390
1391
1392

1393
1394
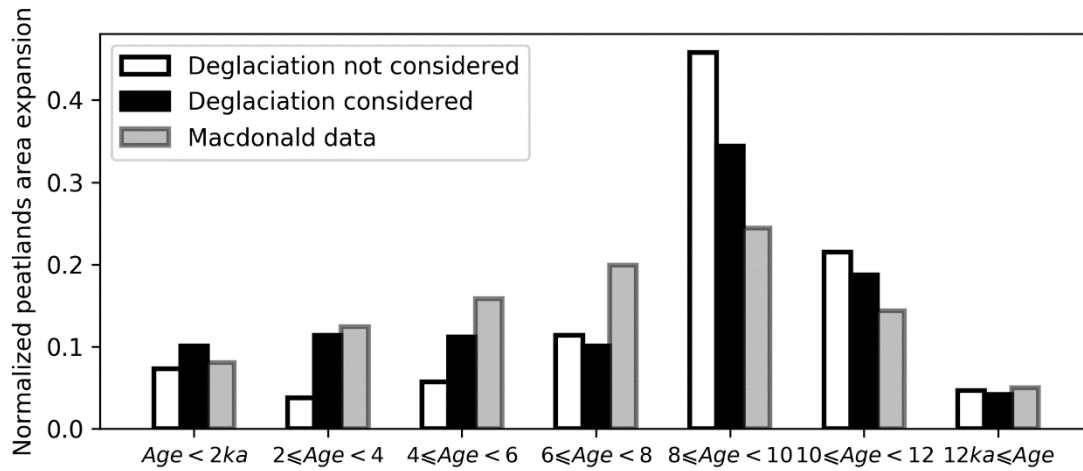
1395 **Fig. 13.** (Grey bars) Percentage of observed peatland initiation in 2000-year bins. Peat
1396 basal dates of 1516 cores are from MacDonald et al. (2006), peat basal age frequency
1397 of each 2000-year bin is divided by the total peat basal age frequency. (White bars)
1398 Percentage of simulated peatlands area developed in each 2000-year bin, deglaciation
1399 of ice-sheets is not considered (the model was run with 6 times SubC, 2000 years each
1400 time). The peatlands area developed in each bin is divided by the simulated modern (the
1401 year 2009) peatlands area. (Black bars) Percentage of simulated peatlands area
1402 developed in each 2000-years bin, pattern and timing of deglaciation are read from
1403 maps in Fig. S5 and Fig. S6.
1404